The ISME Journal (2014), 1–13

www.nature.com/ismej

ORIGINAL ARTICLE

A multitrophic model to quantify the effects of marine viruses on microbial food webs and ecosystem processes

Joshua S Weitz[1,2], Charles A Stock[3], Steven W Wilhelm[4], Lydia Bourouiba[5], Maureen L Coleman[6], Alison Buchan[4], Michael J Follows[7], Jed A Fuhrman[8], Luis F Jover[2], Jay T Lennon[9], Mathias Middelboe[10], Derek L Sonderegger[11], Curtis A Suttle[12], Bradford P Taylor[2], T Frede Thingstad[13], William H Wilson[14,16] and K Eric Wommack[15]

[1]*School of Biology, Georgia Institute of Technology, Atlanta, GA, USA;* [2]*School of Physics, Georgia Institute of Technology, Atlanta, GA, USA;* [3]*Geophysical Fluid Dynamics Laboratory, NOAA, Princeton, NJ, USA;* [4]*Department of Microbiology, University of Tennessee, Knoxville, TN, USA;* [5]*Department of Applied Mathematics, Massachusetts Institute of Technology, Cambridge, MA, USA;* [6]*Department of Geosciences, University of Chicago, Chicago, IL, USA;* [7]*Department of Earth, Atmospheric and Planetary Sciences, Massachusetts Institute of Technology, Cambridge, MA, USA;* [8]*Department of Biological Sciences, University of Southern California, Los Angeles, CA, USA;* [9]*Department of Biology, Indiana University, Bloomington, IN, USA;* [10]*Marine Biological Section, University of Copenhagen, Copenhagen, Denmark;* [11]*Department of Mathematics, Northern Arizona University, Flagstaff, AZ, USA;* [12]*Department of Earth and Ocean Sciences, Department of Botany, and Department of Microbiology and Immunology, University of British Columbia, Vancouver, British Columbia, Canada;* [13]*Department of Biology, University of Bergen, Bergen, Norway;* [14]*Bigelow Laboratory for Ocean Sciences, East Boothbay, ME, USA and* [15]*Delaware Biotechnology Institute, University of Delaware, Newark, DE, USA*

Viral lysis of microbial hosts releases organic matter that can then be assimilated by nontargeted microorganisms. Quantitative estimates of virus-mediated recycling of carbon in marine waters, first established in the late 1990s, were originally extrapolated from marine host and virus densities, host carbon content and inferred viral lysis rates. Yet, these estimates did not explicitly incorporate the cascade of complex feedbacks associated with virus-mediated lysis. To evaluate the role of viruses in shaping community structure and ecosystem functioning, we extend dynamic multitrophic ecosystem models to include a virus component, specifically parameterized for processes taking place in the ocean euphotic zone. Crucially, we are able to solve this model analytically, facilitating evaluation of model behavior under many alternative parameterizations. Analyses reveal that the addition of a virus component promotes the emergence of complex communities. In addition, biomass partitioning of the emergent multitrophic community is consistent with well-established empirical norms in the surface oceans. At steady state, ecosystem fluxes can be probed to characterize the effects that viruses have when compared with putative marine surface ecosystems without viruses. The model suggests that ecosystems with viruses will have (1) increased organic matter recycling, (2) reduced transfer to higher trophic levels and (3) increased net primary productivity. These model findings support hypotheses that viruses can have significant stimulatory effects across whole-ecosystem scales. We suggest that existing efforts to predict carbon and nutrient cycling without considering virus effects are likely to miss essential features of marine food webs that regulate global biogeochemical cycles.
The ISME Journal advance online publication, 30 January 2015; doi:10.1038/ismej.2014.220

Introduction

Viruses infect nearly all forms of cellular life, including the bacteria, archaea and microeukaryotes that are the base of the ocean food web. Empirical studies of viral infection in marine waters (Suttle, 1994; Fuhrman and Noble, 1995; Weinbauer *et al.*, 2003; Wilhelm and Matteson, 2008) and sediments (Middelboe and Glud, 2006; Siem-Jorgensen *et al.*, 2008; Corinaldesi *et al.*, 2010; Umani *et al.*, 2010) have demonstrated that the lysis of hosts by viruses releases cellular material (including carbon and nutrients) back into the microbial loop. Thus, lysis reduces the potential for consumption of microbes by larger organisms and subsequent trophic transfer up the food web (Bratbak *et al.*, 1992; Wommack and Colwell, 2000; Weinbauer, 2004; Suttle, 2007;

Correspondence: JS Weitz, School of Biology, Georgia Institute of Technology, 310 Ferst Drive, Atlanta, GA 30332-0230, USA.
E-mail: jsweitz@gatech.edu
[16]Current address: Plymouth Marine Laboratory, Plymouth, UK.
Received 22 June 2014; revised 15 October 2014; accepted 17 October 2014

Danovaro *et al.*, 2011). This virus-mediated recycling of organic matter has been termed 'viral shunt' (Wilhelm and Suttle, 1999). Indeed, viruses are thought to turn over 20–50% of the marine bacterial community on a daily basis (Fuhrman, 1999). Such estimates were used ~15 years ago to hypothesize that viruses may increase the flux of organic matter through ocean ecosystems when compared with idealized ecosystems without viruses (Fuhrman, 1999; Wilhelm and Suttle, 1999). This hypothesis is supported by manipulative experiments in which viral release of organic matter can have a stimulatory effect on the growth of nontargeted microbial populations (Middelboe *et al.*, 1996; Gobler *et al.*, 1997; Middelboe *et al.*, 2003; Poorvin *et al.*, 2004; Weinbauer *et al.*, 2011; Shelford *et al.*, 2012). However, even if one population is stimulated by the lysis of cells from another population in the short term, the same population may also be susceptible to lysis by other viruses in the community. Hence, the long-term consequences of viral lysis requires consideration of nonlinear feedbacks in a complex system.

Dynamic models of aquatic food webs provide one route to deepen our understanding of the effects and feedbacks of virus–host interactions over the long term. To this end, a limited number of food-web models that include a virus component have been proposed. These models suggest principles by which viruses, through selective lysis, can prevent competitive exclusion and stimulate diversity (Thingstad and Lignell, 1997; Thingstad, 2000) as well as stimulate secondary production (Thingstad, 2000; Miki *et al.*, 2008). Yet, the processes by which viruses mediate carbon and nutrient cycling have still not been integrated into large-scale climate and Earth-system models (Follows *et al.*, 2007; Stock *et al.*, 2014). A key barrier to such integration is that previous models of aquatic food webs that incorporate viruses and nutrients have considered a single kind of limiting resource, for example, phosphate (Thingstad, 2000) or organic carbon (Miki *et al.*, 2008). Here, we propose a step toward integration of viruses into global ecosystem models: a dynamic multitrophic model of a surface ocean microbial ecosystem. The model includes the interactions among organic and inorganic nutrients, phytoplankton (both cyanobacteria and eukaryotic autotrophs), heterotrophic bacteria, zooplankton and viruses—what we term a NPHZ-V model. Because of the *in silico* nature of the study, we are able to ask: 'how do ecosystems differ with vs without viruses?' As we show, despite killing their hosts, virus-mediated recycling of nutrients is associated with stimulatory effects on ecosystem function that lay on a continuum between exclusive bottom-up or top-down control.

Materials and methods

The NPHZ-V model considers the coupled dynamics of biological populations and nutrients in the euphotic zone of the surface ocean (see Figure 1). The biological populations represent functional groups, including three groups of microbes: heterotrophic bacteria (H), cyanobacteria (C) and eukaryotic autotrophs (E), three groups of viruses (that each exclusively infect only one of the three microbial groups, V_H, V_C and V_E, respectively) and a general zooplankton group (Z, that can feed on all three types of microbes, analogous to a composite nano-/micro-zooplankton functional group). The nutrients considered are the concentration of bioavailable organic (x_{on}) and inorganic matter (x_{in}). The entire model utilizes nitrogen as a common currency, that is, organisms of each population have the same, fixed stoichiometry (see 'Results and discussion' section for further treatment of this issue). We refer to densities of all biological populations in units of cells l^{-1} and nutrient concentrations in units of $\mu mol\, l^{-1}$. The resulting coupled system of nonlinear, ordinary differential equations are presented in the Supplementary Appendix. We summarize the meaning of each process below.

Heterotrophic growth
Heterotrophic bacteria take up dissolved organic matter via a Michaelis–Menten saturating response. Organic matter is allocated to anabolic (growth) and catabolic (respiration) processes assuming a fixed growth efficiency.

Cyanobacterial and eukaryotic phytoplankton growth
Both groups of autotrophs take up inorganic nutrients via a Michaelis–Menten saturating response. This inorganic matter is fixed as biomass.

Cellular loss and respiration
Microbes undergo first-order decay terms because of release of organic cellular matter and respiration.

Viral lysis of microbes
For each virus group, successful infections with their target hosts occur at a rate proportional to the product of host and virus densities. Infections lead to the death of hosts and the release of a virus 'burst'. Lysis includes the release of x_{on}, assumed to be the difference between the nutrient content of hosts and the total nutrient content within the released viruses.

Viral decay
Viruses decay at a constant rate proportional to their densities. The nutrient content of decayed viruses is regenerated as organic matter.

Zooplankton grazing
Zooplankton consume each microbial population at a rate proportional to the product of the densities of zooplankton and each microbial population. Consumed

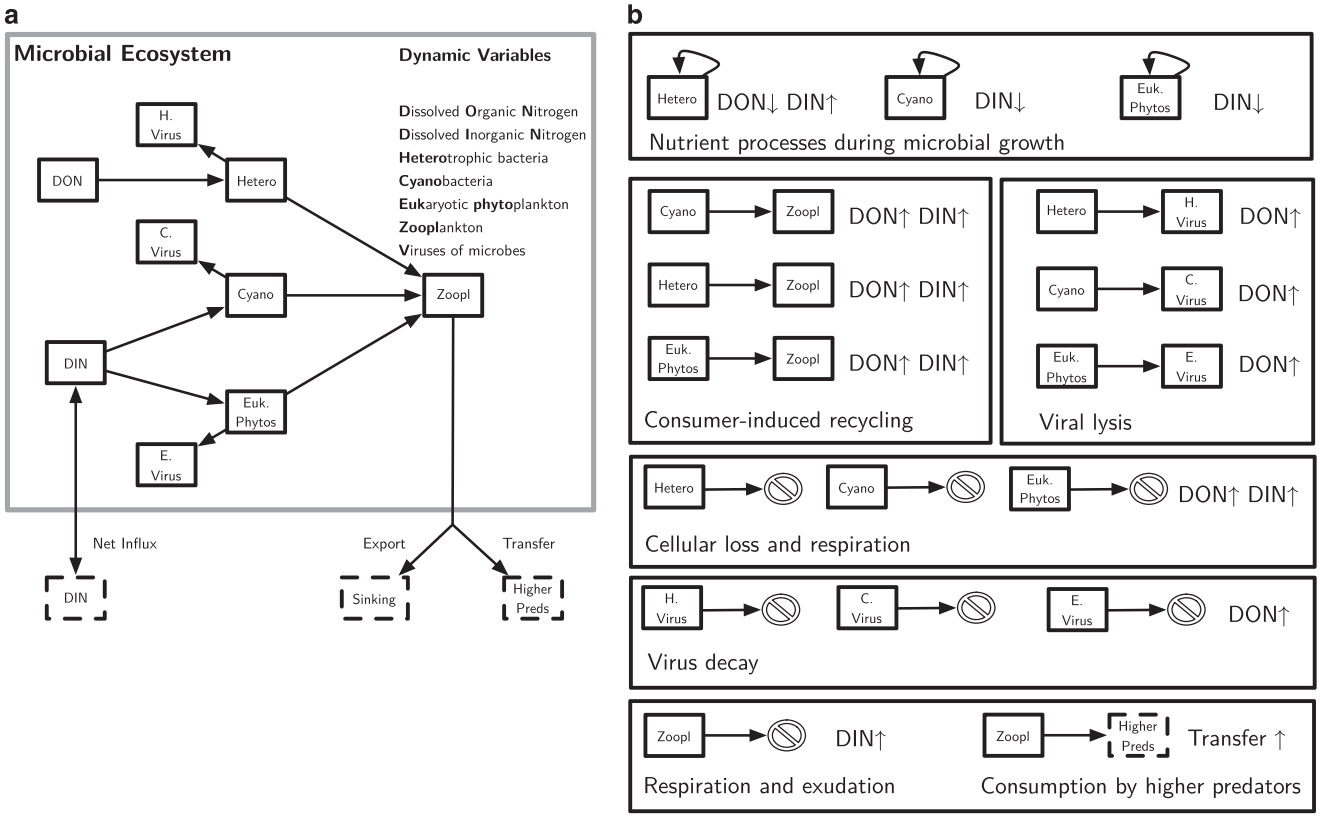

Figure 1 Schematic of the NPHZ-V model. (**a**) Interactions between populations and nutrients where arrows denote the flow of materials in the system. Note that decay processes are not depicted and the secondary effects on nutrients are depicted in (**b**). (**b**) Nutrient cycling in the system. Each of the different processes affect the levels of dissolved organic nitrogen (DON) and dissolved inorganic nitrogen (DIN), where the symbols ↑ or a ↓ denote whether a given process increases or decreases that particular pool, respectively.

biomass is subject to an ingestion efficiency that takes into account sloppy feeding (leading to release of organic matter) and growth efficiency (biomass allocated to growth vs respiration).

Zooplankton respiration
Total respiration consists of a basal component proportional to the biomass of zooplankton and an active component proportional to ingestion.

Zooplankton removal
Zooplankton biomass is 'removed' from the system at a rate proportional to the squared density of zooplankton. This nonlinear removal rate implicitly models the effect of predation on zooplankton, assuming that the number of these unresolved predators scales with the number of the zooplankton prey (Stock *et al.*, 2014). A fraction of the removed zooplankton biomass is exported from the system (for example, as pellets or other sinking material) and a fraction is considered to have been transferred to higher trophic levels.

Inorganic nutrient exchange
Exchange of water between the surface and subsurface leads to a change in inorganic matter concentration proportional to the difference between the surface concentration and subsurface concentration. Although the surface concentration of inorganic matter varies dynamically in the model, the subsurface concentration is held fixed.

Results and discussion

Virus–host interactions permit multitrophic coexistence
We derived the expected steady state including the coexistence of all biological populations. Such coexistence occurs for a wide range of parameters (see Supplementary Appendix for conditions), that is, coexistence does not require fine-tuning of parameters. Hence, we predict that the three functional types of viruses can persist and indeed (as we later show) promote coexistence in this multitrophic system. The key insight that enables the present derivation is that viruses, in this model, are assumed to exclusively lyse hosts. In the initial formulation, lysis of hosts is modeled as a type-I functional response, that is, proportional to the product of host and virus densities (Murray and Jackson, 1992). The burst size is equivalent to the total number of released viruses minus the virus necessary to initiate the infection. Virus population densities

reach steady state when new viral production is balanced by virus particle decay. Both of these terms depend linearly on virus densities, implying that microbial host densities must be limited by viral lysis and not by a combination of resource availability and zooplankton grazing. This result is consistent with long-standing theory (Carpenter *et al.*, 1985) and observations (Pace *et al.*, 1999) on the potential of trophic cascades in multitrophic systems in which addition of a top predator switches control of consumer biomass from bottom-up to top-down. Similar observations have been made in models specifically developed for the study of virus–host interactions in the oceans (for example, the Kill-the-Winner model; Thingstad and Lignell, 1997; Thingstad, 2000). However, within food-web models, the nature of trophic cascade depends on the type of regulation and even the functional response of consumers to resources (Heath *et al.*, 2014), suggesting that similar analysis of variations in the present model are warranted.

Coexistence in this model can occur either via a fixed point equilibrium or via an oscillatory steady state (see Supplementary Figure S1 for two examples). Such behavior suggests that there likely exists a Hopf bifurcation in the system, that is, a change in parameters destabilizes a fixed point equilibria so that the steady state becomes a limit cycle (Strogatz, 1994). We have not formally derived the criteria for the bifurcation given the complexity of the model. We note that prior analysis of models of virus–host interactions with implicit resources (but an explicit infected host class) (Beretta and Kuang, 2001) as well as models with explicit time delays between infection and lysis (Levin *et al.*, 1977) also have yielded oscillatory dynamics at steady state. Hence, our multitrophic model further supports claims that oscillatory dynamics of complex marine ecosystems may be promoted because of endogenous feedbacks (here, including virus–host interactions and virus-mediated recycling), in addition to exogenous factors, for example, cyclical forcing associated with seasonality. The finding of stable coexistence raises the question: how do the population densities vary with respect to changes in parameters?

Steady-state densities predicted by model dynamics

We systematically investigated the extent to which realistic features of microbial surface ocean communities could emerge within the model structure. First, we performed a global sensitivity analysis by varying all parameters independently. The parameter space was sampled with 10^6 model replicates using a Latin hybercube sampling scheme (McKay *et al.*, 1979), using uniform distributions across logarithmically stratified uncertainty ranges (Thingstad, 2000; Miki *et al.*, 2008; Williams and Follows, 2011) (see Supplementary Appendix for more details). We found that 4366 ($\approx$0.45%) of the 10^6 model simulations led to coexistence among all types—we denote these parameter combinations as 'feasible'. We consider the identification of $\sim 4.5 \times 10^3$ feasible model replicates to be substantial given the nonlinearity of the model and the high dimensionality of the underlying parameter space. The range of densities of populations and nutrients predicted in the Latin hybercube sampling coincide with biologically plausible population and nutrient levels (see Figure 2). We also classified the local stability of equilibrium points via a systematic examination of the eigenvalue spectra of all feasible coexistence points among 10^6 parameter combinations sampled via Latin hybercube sampling. We find that a majority ($\approx$90%) of points correspond to locally stable fixed points, whereas a minority ($\approx$10%) of points correspond to unstable spirals. Hence, stable coexistence in the model is both generic and compatible with observed densities of populations, organic and inorganic nutrients in the surface oceans. However, exceptions do occur, for example, some parameters lead to coexistence with seemingly unrealistic subsets of predicted densities and/or concentrations such as cyanobacteria at densities exceeding 10^{10} cells l^{-1}. It is well known that parameters within model representations of complex multitrophic models often require further refinement to reach (realistic) steady states. Indeed, the present model includes 9 dynamic equations and 38 parameters for which manual optimization was considered infeasible.

Instead, we developed an automated procedure to search through the 38-dimensional parameter space while minimizing the log-squared difference in predicted model densities relative to a 'target'. Log-square differences weight the log ratio of deviations rather than absolute deviations. The use of log-square differences is appropriate when reconciling candidate and target predictions whose values differ across multiple orders of magnitude and in fundamental units. The target densities used in this procedure denote an idealized marine surface ecosystem (Table 1). In addition, the optimization

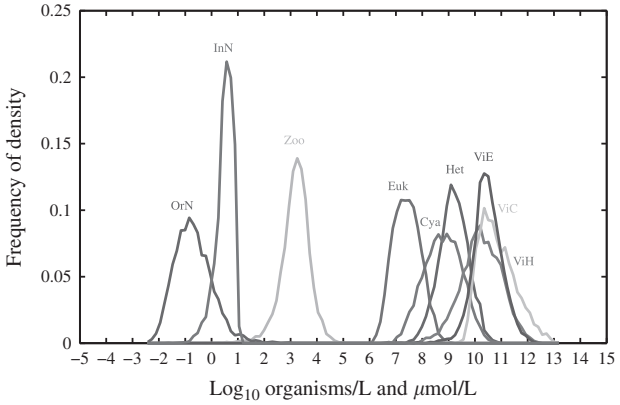

Figure 2 Variation in model output via a Latin hybercube resampling (LHS) of parameter space. Parameter space for LHS analysis is documented in the Supplementary Information.

procedure also included the following system features: total virus to bacterium ratio (10:1) and the fraction of mortality of *H*, *C* and *E* due to viruses (50%, 25% and 10%, respectively). Full details of the procedure are available in the Supplementary Appendix. The results of this optimization procedure are twofold: (1) a set of parameter combinations and (2) a set of predicted population densities. We then ranked each parameter combination according to the weighted deviation of model output to the target. The distribution of predicted population densities and ecosystem features associated with the top 5% of all 'targeted' parameter combinations (218 distinct model replicates in total) can be seen in Figure 3. The features include relationships that have been empirically observed, including ratios of total viruses to bacteria on the order of 10:1 and the relative importance of viruses to cellular mortality ranging from marginal to dominant. For this target, 95% of the 218 top-performing model replicates were found to be locally stable (see Supplementary Figure S2). The parameter combinations associated with this optimization procedure can be seen in Supplementary Figure S3. These 218 parameter combinations that yield realistic microbial population densities and nutrient concentrations reflect an emergent feature of the model. Identification of replicates was enabled by our nonlinear optimization strategy to search a high-dimensional parameter space. As has been noted in the case of other models of nonlinear systems many of the parameters are relatively 'sloppy', that is, changes in their values can be consistent with similar model outputs, whereas a few are stiff, that is, parameters must be narrowly constrained to yield similar model outputs (Gutenkunst *et al.*, 2007). This notion applies here (see Supplementary Information and Supplementary Figures S6 and S7). For example, parameters associated with cyanobacterial interactions emerge as the stiffest, when using the top-performing parameter set as a reference. Moving forward, the relative stiffness of parameters presents one opportunity for testing putative mechanisms underlying model predictions. In summary, the NPHZ-V model, when suitably parameterized, is consistent with the emergence of multitrophic coexistence in which population densities, nutrient concentrations and ecosystem features are simultaneously compatible with biological variation in the marine surface environment.

Table 1 Target densities and concentrations used in the optimization procedure

Pool	*Variable*	*Target density*	*Units*
Heterotrophs	H*	2×10^8	Cells l^{-1}
Cyanobacteria	C*	2×10^8	Cells l^{-1}
Eukaryotic autotrophs	E*	2×10^6	Cells l^{-1}
Zooplankton	Z*	5×10^4	Cells l^{-1}
Viruses of H	V_H^*	2×10^9	Particles l^{-1}
Viruses of C	V_C^*	2×10^9	Particles l^{-1}
Viruses of E	V_E^*	2×10^7	Particles l^{-1}
Organic nitrogen	x_{on}^*	5	μmol l^{-1}
Inorganic nitrogen	x_{in}^*	0.1	μmol l^{-1}

Marine microbial densities based on variation reported for total cyanobacteria populations, exceeding 10^8 cells l^{-1} (Johnson *et al.*, 2006), assuming similar concentrations of heterotrophic bacteria. Densities of eukaryotic autotrophs are in the range of 2×10^6 cells l^{-1}, during nonbloom conditions (Schartau *et al.*, 2010), with the same study reporting total zooplankton exceeding 10^4 cells l^{-1} and, for some groups, exceeding 10^6 cells l^{-1} (Schartau *et al.*, 2010). Total virus counts are centered in the range of 10^8–10^{11} particles l^{-1} (Danovaro *et al.*, 2011; Breitbart, 2012) and are set here to be 10-fold higher than their corresponding microbial hosts (Suttle, 2007). Dissolved inorganic nitrogen is depleted in the ocean surface, with concentrations of <1 μmol l^{-1} typical in the subtropics (Williams and Follows, 2011), in contrast to dissolved organic nitrogen that is enriched in the ocean surface with concentrations in the range of 2 to 7 μmol l^{-1} (Letscher *et al.*, 2013). Population densities and nutrient concentrations vary spatiotemporally, often deviating from the current set of target densities; other values could also be used in the targeted optimization procedure.

Viral effects on community structure

Having established parameters within the NPHZ-V model that yielded biologically plausible coexistence, we evaluated the effects that viruses have on surface ocean ecosystems by comparing steady-state output and fluxes in systems with and without viruses while keeping all other parameters fixed. We performed this comparison with the entire suite of 4366 feasible parameter combinations and with the 218 targeted parameter combinations identified via a nonlinear optimization procedure. In comparing community structure to an ecosystem without viruses, we first solved the model while setting all virus densities to zero (see Supplementary Appendix). As we show in the Supplementary Appendix, the current model structure does not permit the fixed point coexistence of cyanobacteria and eukaryotic autotrophs unless viruses are present. This is a consequence of the fact that, in the present model without viruses, both the *C* and the *E* populations compete for the identical resources (x_{in}) and are subject to the same predator (Z) that itself is subject to implicit predation. Hence, coexistence is not expected because of competitive exclusion (Armstrong and McGehee, 1980), unless *C* and *E* are subject to clade-specific parasites (for example, viruses). Coexistence would have been possible even without viruses, had we refined the model to include distinct nutrient sources, selective (or nonlinear) grazing or other forms of heterogeneity. Nonetheless, given the current model structure, this qualitative difference between steady states helps to strengthen support for the notion that viruses, even when strictly deleterious to host cells they infect, can have system-wide effects, including increasing biodiversity. The need to consider the role of parasites in food webs has only recently been highlighted (Lafferty *et al.*, 2008), with some evidence (predominantly within aquatic food webs associated with coastal habitats) suggesting that parasites have the potential to increase diversity (Dunne *et al.*, 2013).

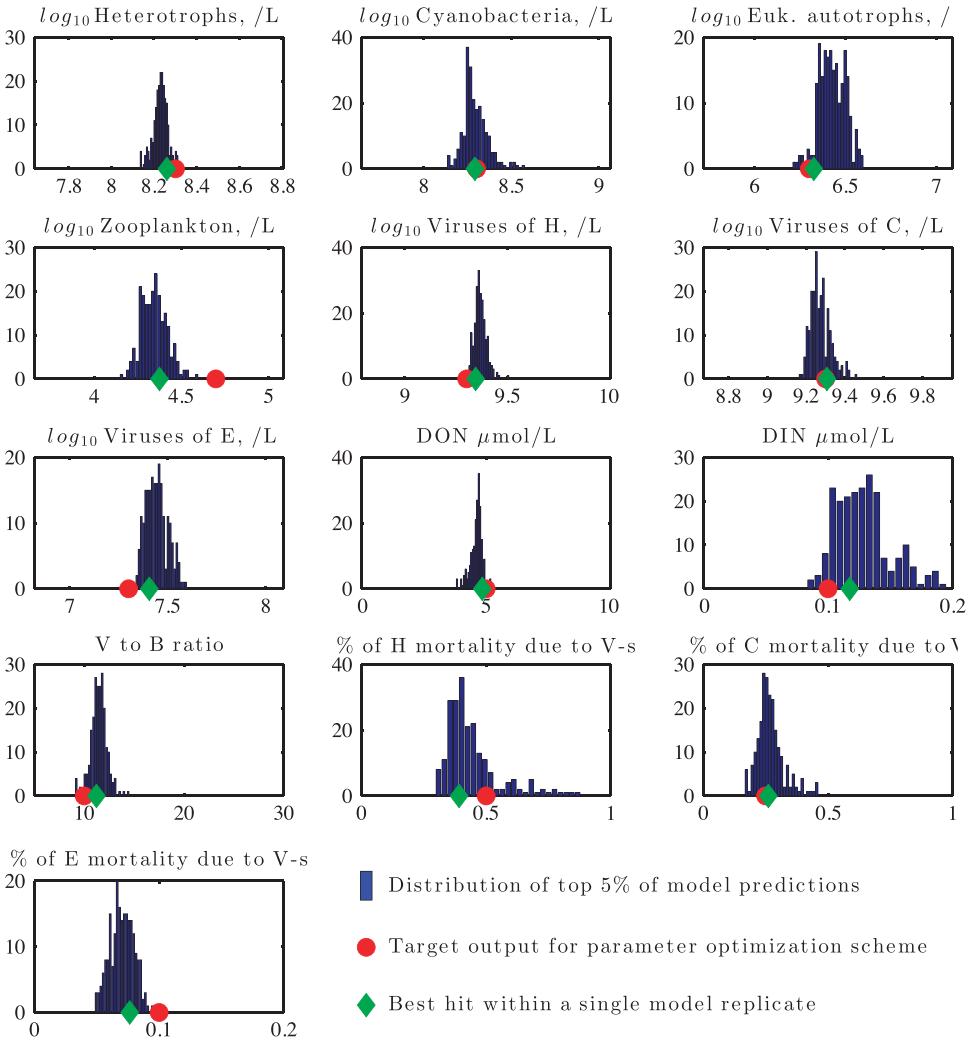

Figure 3 Distributions of community properties obtained via nonlinear optimization. The distribution correspond to the top 5% of model feature output (blue histogram) as compared with target values (red circle), along with the properties associated with the best ranking model replicate (green diamond). The number of cases (out of 218 top-performing model replicates) are noted on the y axis.

We can compare predictions of community structure with viruses with those without viruses by focusing on direct comparisons of H, C, Z, x_{on} and x_{in} within models where $C^* > 0$ but $E^* = 0$. The '*' denotes that the associated density or concentration is at steady state. Similarly, we utilize the results of models where $E^* > 0$ but $C^* = 0$ to compare with predicted densities of E with viruses. Note that our comparisons include results using the full range of parameter combinations (that is, the feasible replicates) and the optimized set (that is, the targeted replicates). In general, we find that viruses increase steady-state concentrations of inorganic nutrients in the system (see Figure 4). For example, models with viruses lead to steady-state concentrations of inorganic nitrogen between 0.1 and 10 $\mu mol\, l^{-1}$ whereas without viruses, the steady states are characterized by inorganic nitrogen levels between 0.001 and 0.1 $\mu mol\, l^{-1}$. We also find that viruses generally, but not inevitably, increase organic nutrients in the system. This increase in nutrients when a top predator is added is characteristic of the switch from a bottom-up system (that is, nutrient limited) to top-down system (that is, predator or parasite limited) (Hunter and Price, 1992). We also find that the effect sizes differ between the feasible and targeted replicates—this is expected, given that targeted replicates are consistent with a much narrower distribution of biomass, nutrients and ecosystem features than are the feasible replicates.

There are also emergent properties arising from the model that defy conventional intuition associated with a shift from bottom-up to top-down control. One might have expected that inclusion of viruses would inevitably decrease the density of heterotrophic bacteria. To the contrary, we find that heterotrophic bacteria densities typically increase by a factor of 5 in ecosystems with viruses vs those without (while holding all other parameters fixed). With viruses, heterotrophic density is top-down controlled and determined by the rates of virus decay relative to the product of virus–host contact

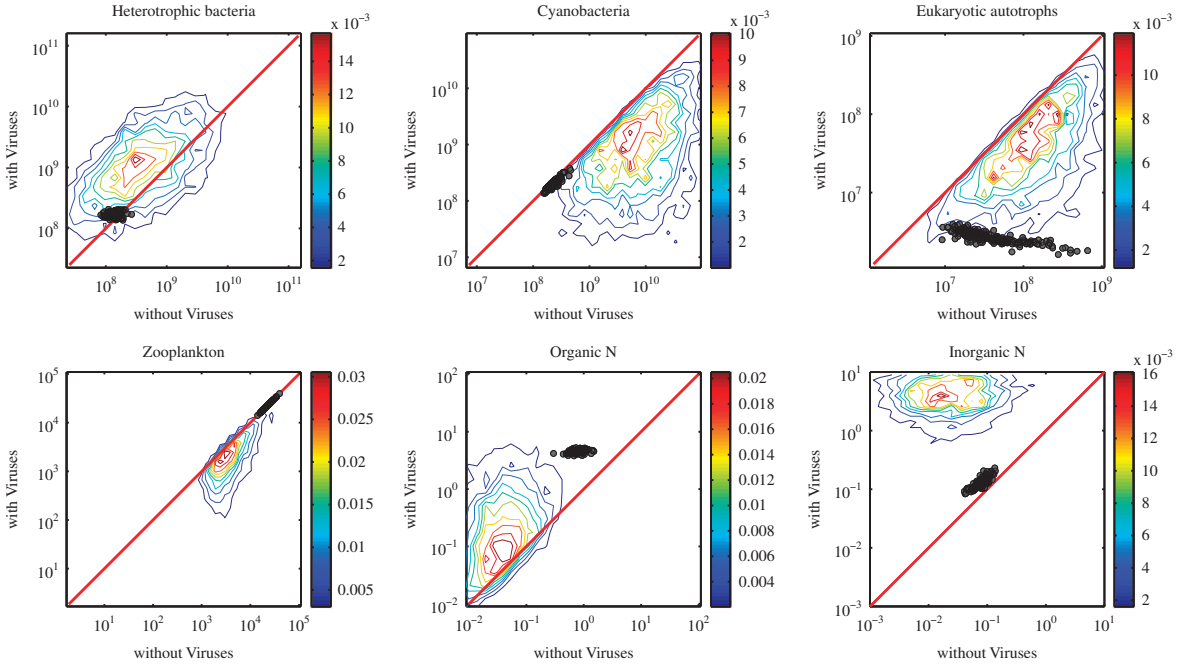

Figure 4 Comparison of steady-state concentrations with and without viruses. The colored lines denote contours of equal probability among 4366 model replicates (obtained via Latin hybercube sampling (LHS)) that yielded a coexistence equilibrium (see main text; histograms conducted in logarithmic space as input for contour analysis). The circles denote comparisons for the 218 model replicates identified as part of the targeted nonlinear optimization procedure (see main text). The red line denotes the 1:1 line. Comparisons to results without viruses are restricted to model results where $C^* > 0$ with the exception of the comparison of eukaryotic autotrophs. In each panel, viruses increase/decrease the pool of interest, as compared with ecosystems without viruses, when points (or contours) lie above/below the red line.

rates and burst size. Without viruses, heterotrophic density is limited by a combination of zooplankton grazing and organic matter availability. Hence, the effect of including viruses in this surface microbial ecosystem model suggests that they can have a net stimulatory effect, via an indirect route, on the populations that they directly inhibit. As far as we are aware, this issue is underexplored in the study of host–viral interactions and, more generally, in the study of the role of parasites in ecosystem dynamics (Lafferty *et al.*, 2008). Similarly, we found that although the total density of either the cyanobacteria or eukaryotic phytoplankton decreases in abundance when viruses are added (see Figure 4) their *combined* pool size increases in abundance when viruses are added. This observation raises the question of how viruses change the total amount of nitrogen in the distinct pools.

We directly evaluated the change in the partitioning of biomass in the ecosystem by comparing the nitrogen content within the nutrient pools, x_{on} and x_{in}, and within each population: $q_H H$, $q_C C$, $q_E E$, $q_Z Z$ and $q_V V_{H/C/E}$, where q denotes the nitrogen content per organism type (noted in the subscript). Figure 5 depicts the pool size corresponding to each population and nutrient type for the 218 targeted model replicates identified earlier. As is apparent, the total nitrogen concentration ($x_{on} + x_{in}$) in the environment increases when viruses are included. A full examination of the response of the surface microbial ecosystem (and its total biomass) to the addition of viruses depends on the particular form of closure implicit in this model. Nonetheless, such stimulatory effects need not have occurred, given that all microbial groups were subject to viral lysis. It is the feedback between lysis and nutrient pools that enabled the system-wide stimulation to take place. However, as anticipated from the pairwise comparisons in Figure 4, we observed significant changes in the relative abundance of pool sizes in each population when discounting for the change in the total nutrients bound in the surface microbial ecosystem ($P = 10^{-10}$, Kolmogornov–Smirnov pairwise test). This result holds even for the case of zooplankton that do not change significantly in total biomass for the targeted parameter sets (see Figure 4). However, because of the overall increase in total biomass, the zooplankton decrease significantly in their relative abundance when viruses are included in the ecosystem (as is apparent in Figure 5). Moreover, as previously noted, the total pool size in the autotrophs increases when viruses are added (similar to the increase in heterotrophic biomass). Hence, viruses can alter both the total size of the microbial ecosystem and the relative partitioning within it.

Viral effects on ecosystem functioning

We analyzed ecosystem-level effects of viruses, using the same sets of feasible and targeted parameters as

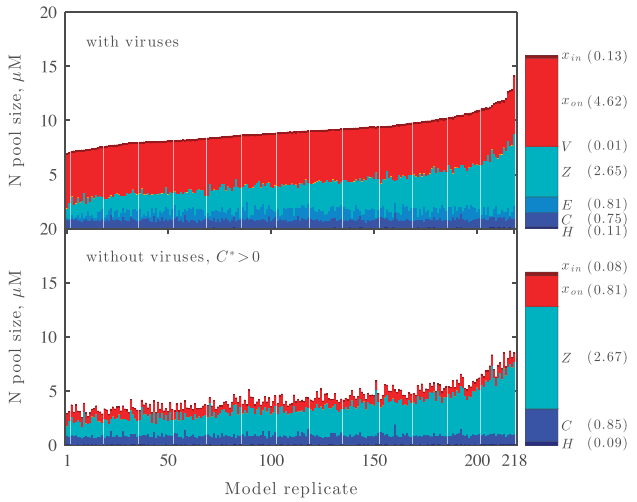

Figure 5 Viral effects on community structure. The left panels (top and bottom) are stacked histograms of the concentration of nitrogen (N, in units of μM) partitioned in the different variables, H, C, E, Z, V (all types), x_{on} and x_{in}. The 218 stacked histograms correspond to each of the 218 parameter sets identified in the nonlinear optimization procedure described in the main text. The parameter sets were ordered based on the predicted total density of nitrogen (either organic or inorganic) at steady state within the specified variables. Hence, the top panel shows increasing total height. The 218 stacked histograms in the bottom-left panel show the expected average partitioning in ecosystems with the same parameters, although without viruses. The legend on the right includes information on both the color associated with each variable and the average concentration of N partitioned in that variable.

explained in the previous section. We considered three classes of effects whose magnitude of flux might differ in ecosystems with viruses vs those without viruses: (1) organic matter regeneration, (2) transfer to higher trophic levels and (3) net primary productivity. We defined organic matter regeneration as the total flux of processes that return matter into the organic matter pool as a consequence of viral lysis of hosts and zooplankton grazing of microbes. We defined the transfer to higher trophic levels to be a fraction (p_{ex}) of the zooplankton biomass loss (that is, as consumed by higher trophic predators). We defined the net primary productivity to be the total rate of inorganic matter fixed by cyanobacteria and by eukaryotic phytoplankton. Each of these fluxes (in units of μmol l^{-1} $days^{-1}$) is calculated at steady state in an ecosystem model with vs without viruses. We find that ecosystems with viruses exhibit (1) increased organic matter recycling, (2) reduced transfer to higher trophic levels and (3) increased net primary productivity (see Figure 6). Moreover, primary productivity in the targeted model replicates, in units of mg C m^{-2} $days^{-1}$, have a mean of 1130 with s.d. of 270 (see Supplementary Figure S4). As a reference, note that empirical estimates of net primary productivity of 1140 (in the same units) have been derived for an Equatorial Pacific upwelling (Barber *et al.*, 2001). The present model results are on the high end when compared with simulated net primary productivity for a multitrophic model without viruses, ranging from 200 to 1000 mg C m^{-2} $days^{-1}$ (Stock *et al.*, 2014). As we note below, the present model likely overestimates primary productivity because of the assumption of a highly efficient microbial loop.

Viral-induced stimulation of the productivity of cyanobacteria was previously hypothesized to be a potential consequence of the viral shunt (Fuhrman, 1999; Wilhelm and Suttle, 1999). More generally, multiple groups have reported that viral lysis can stimulate the productivity of nontargeted populations in the short term (Middelboe *et al.*, 1996; Gobler *et al.*, 1997; Middelboe *et al.*, 2003; Poorvin *et al.*, 2004; Weinbauer *et al.*, 2011; Shelford *et al.*, 2012). Here, such effects are shown to be consistent with anticipated nonlinear feedbacks and nutrient dynamics of a multitrophic surface microbial ecosystem model over the long term, including both inorganic and organic nutrient pools. Note that although the targeted model replicates do exhibit reduced transfer to higher trophic levels, the reduction is minimal (see the near 1:1 correspondence in Figure 6 in the upper-right panel). This phenomenon is, in part, a consequence of the assumption of a highly efficient microbial food web. Note that the present model only considers the exchange of inorganic nitrogen across the nutricline (and therefore no loss of nutrients directly from the microbial pools). The only other loss term that can balance this exchange is associated with the consumption of zooplankton. Here, the consumption of zooplankton is implicit, that is, proportional to Z^2, hence the steady state Z^* must be nearly identical to that in a virus-free model, so long as x_{in}^* is much smaller in the system than below the nutricline. In this limit, transfer to higher trophic levels and export will be nearly identical, with or without viruses. The extent to which the microbial loop generates export depends on its efficiency which is affected by microaggregation, direct sinking of particulate organic matter (some of which are generated by viral lysis of hosts) and downward mixing among other potential (Lomas and Moran, 2011; Williams and Follows, 2011; Stock *et al.*, 2014). These mechanisms will likely prove relevant if Earth Systems models are to include virus–host interactions that would otherwise enhance the efficiency of the microbial loop.

Finally, recall the observation that steady-state densities of each group of primary producers are predicted to decrease when viruses are present. However, both the total combined biomass of autotrophs and net primary productivity are predicted to increase. This apparent paradox is resolved by observing that in systems with viruses, there is greater recycling of materials that increases the availability of inorganic nutrients (in part stimulated by remineralization by a larger heterotrophic pool), hence increasing primary productivity on a per-cell basis. We evaluated this hypothesis directly by estimating the turnover rate of cyanobacteria in

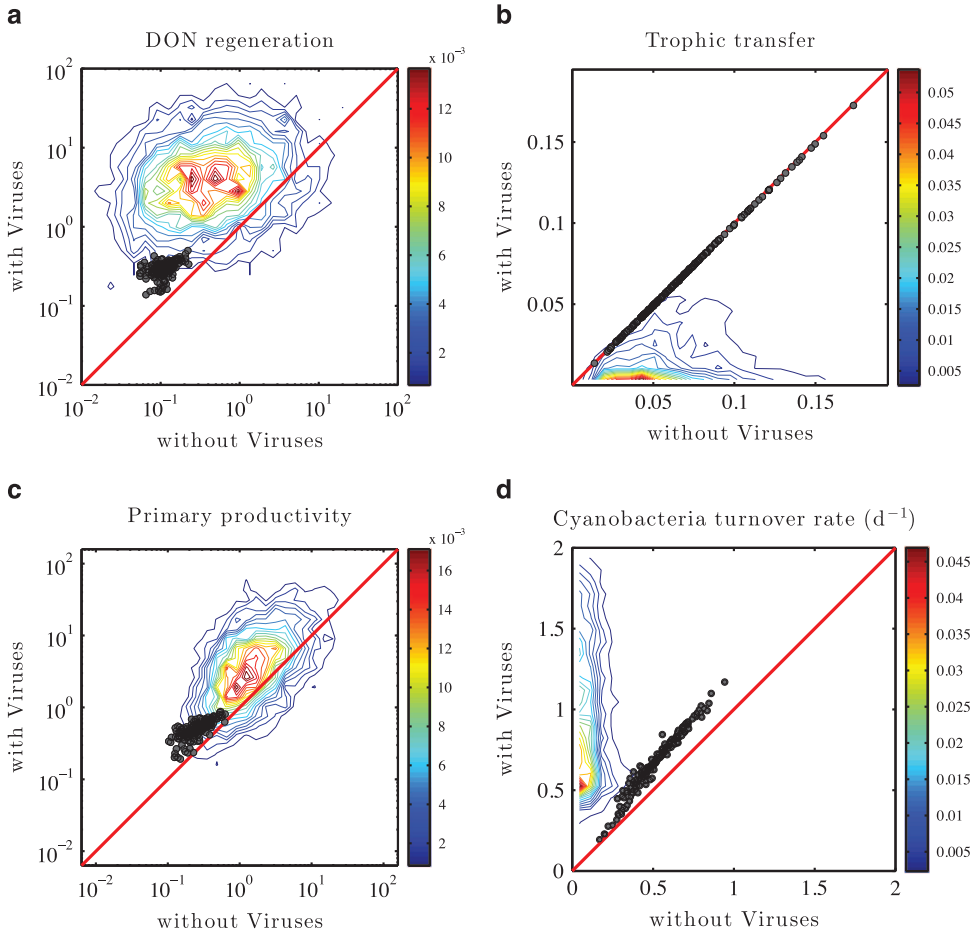

Figure 6 Ecosystem functioning effects of viruses, including (**a**) DON regeneration; (**b**) trophic transfer; (**c**) primary productivity; (**d**) cyanobacteria turnover rate. The contour lines represent the probability distribution of pairwise comparisons for the 4366 model replicates identified by Latin hybercube sampling (LHS; see main text). The circle denote comparisons for the 218 model replicates identified as part of the targeted nonlinear optimization procedure (see main text). The red line denotes the 1:1 line and contours provide information on the relative density of observed point pairs (histograms conducted in logarithmic space for two left panels and in linear space for two right panels as input for contour analysis). All axes denoting ecosystem fluxes are in units of μmol(l days) $^{-1}$, whereas the axes for cyanobacterial turnover are in units of days.

ecosystems with and without viruses. As anticipated, the cyanobacteria turnover rate increases with viruses when compared with ecosystems without viruses (see Figure 6d). Importantly, the turnover rates of the targeted model replicates correspond to cyanobacterial residence times ranging from 0.7 to 3.3 days, with a median of 1.5 days. The relationship between residence times and steady-state densities for all biological populations and nutrient pools within the targeted model replicates can be seen in Supplementary Figure S5. In summary, viruses have the effect of stimulating the ecosystems by increasing DON regeneration, increasing primary productivity (and cyanobacterial turnover) and potentially decreasing transfer to higher trophic levels.

Conclusions

We have developed a dynamic model representing interactions within the microbial component of a surface ocean ecosystem. The NPHZ-V model developed here combines principles of NPZ models with a single limiting nutrient (Legovic and Cruzado, 1997; Klausmeier *et al.*, 2004) with models of virus–host dynamics (Levin *et al.*, 1977; Thingstad and Lignell, 1997; Thingstad, 2000), with explicit consideration of virus-mediated recycling (Menge and Weitz, 2009), but without explicit consideration of the infected state (Beretta *et al.*, 2002). These simplifications enabled us to make specific predictions on the range of effects that viruses have on microbial ecosystems in marine surface waters. Given suitable parameterization, coexistence among each population occurs with steady-state densities in line with observed variation of populations and nutrients in the surface ocean. We further isolated the effect of viruses by comparing model dynamics with and without the inclusion of virus populations. In doing so, we found that ecosystems with viruses exhibit decreased abundance of zooplankton and increased abundance of organic and inorganic nutrients. These results would seem to be consistent with a shift from bottom-up (that is, nutrient limited) to top-down (that is, parasite limited)

ecosystems. Yet, we also found that ecosystems with viruses could exhibit increased total biomass among heterotrophic bacteria and among autotrophs (combining the cyanobacteria and eukaryotic pools). We suggest this increase is a direct result of viral-induced recycling of nutrients. Indeed, we find that ecosytsem functioning is qualitatively changed when viruses are added. For example, ecosystems with viruses exhibit increased regeneration of nutrients, increased primary productivity (and corresponding cyanobacterial turnover rates) and decreased transfer of matter to higher trophic levels. These findings lend further quantitative support to prior hypotheses on the potential for viral-associated effects on global nutrient cycles (Fuhrman, 1999; Wilhelm and Suttle, 1999; Suttle, 2005; Brussaard *et al.*, 2008; Weitz and Wilhelm, 2012).

The combination of analytical results and systematic analysis of variation in model output with respect to parameter variation provides significant support for the generality of our claims. Nonetheless, caution is warranted. Given the complexity of the model, one may ask: how does model output depend on the functional form of model interactions and even the diversity of biological populations, rather than exclusively on parameter variation given a fixed model? We cannot yet provide a complete answer to this question. Nonetheless, our choice of model structure reflects an intent to extend core models of marine microbial communities with minimal virus–host interactions. Hence, whereas explaining complex phytoplankton and nutrient dynamics in the absences of viruses may require consideration of these factors, it is not yet known how much of the unexplained variability in steady states, dynamics and responses could be attributed to virus–host interactions and virus-mediated recycling of nutrients. The *in silico* comparisons of ecosystem dynamics with and without viruses provide one step toward such a comparison. However, part of the difficulty in comparing models lies in the fact that even the relatively simple model structure examined here included 38 parameters. Hence, substantial variation in model output is possible given alternative parameterizations. Moreover, many parameter combinations led to estimates of densities and fluxes simultaneously in line with multiple observations from marine surface waters as well as novel predictions. Moving from testing predictions to testing parameters (and functional interactions) is an important challenge in reconciling complex models with data (Gutenkunst *et al.*, 2007).

In moving forward, the current model provides a foundation for future explorations of the range of consequences associated with alternative fates of infected cells and virus particles in a systems context. In doing so, we highlight multiple priorities. First, it is essential to extend the current model to link increasingly strain-resolved information on microbial and viral diversity (Breitbart *et al.*, 2002; Edwards and Rohwer, 2005; Allen *et al.*, 2011) and interactions between viruses and their hosts (Flores *et al.*, 2011; Deng *et al.*, 2012; Weitz *et al.*, 2013) the aggregated representation of virus–host interactions and nutrient feedbacks presented here (see the example of a calibrated model for dynamics including viruses of the algae *Phaeocystis globosa*; Ruardij *et al.*, 2005). Strain-specific interactions also include the change in host physiology that occurs during infection, whether preceding lysis (Lindell *et al.*, 2007; Ankrah *et al.*, 2014) or during long-term associations with hosts, for example, lysogeny (McDaniel *et al.*, 2008). Such extensions are analogous to the expanded representations of phytoplankton and zooplankton in terms of size-structured and/or functional type groups (Follows *et al.*, 2007; Stock *et al.*, 2014). Next, it is noteworthy that virus–host interactions unfold in a dynamic landscape of multiple nutrients, both organic and inorganic. A recent study suggested that virus lysis may be limited by phosphorus availability within hosts (Jover *et al.*, 2014). Hence, viral lysis may transform (not just shunt) elements back into the microbial loop (Weitz and Wilhelm, 2012). Quantifying the effects of such elemental transformations requires integrating realistic ecological stoichiometry into the present model context (Sterner and Elser, 2003). In doing so, it will also be necessary to consider phytoplankton growth as limited by availability among multiple nutrients, rather than a single nutrient (Legovic and Cruzado, 1997; Klausmeier *et al.*, 2004). The emergent ratios of organic elements have been shown to vary with latitude in the global oceans that may be driven by variation in the availability of inorganic nutrients (Martiny *et al.*, 2013) Finally, there is a delay—the latent period—between infection and lysis, currently omitted from the model framework. Reported latent periods for marine viruses vary from less than an hour (Raytcheva *et al.*, 2011) to dozens of hours (or more) (Suttle and Chan, 1993; Jacobsen *et al.*, 1996; Lindell *et al.*, 2007). Delays between infection and lysis can destabilize model predictions of population dynamics given a single virus–host pair (Levin *et al.*, 1977; Smith and Thieme, 2012). Incorporating such delays into a multitrophic model requires resolving the likely heterogeneous distribution of latent periods in a given community (for example, see alternative representations of the delay in the models of Beretta and Kuang, 2001; Bonachela and Levin, 2014). In addition, inclusion of a pool of infected host cells also requires improved quantification of ocean processes, such as changes in nutrient uptake within infected cells (Bidle and Vardi, 2011; Ankrah *et al.*, 2014) and grazing of infected cells by zooplankton.

We are aware of only one other attempt to integrate viruses into a NPZ framework, including both organic and inorganic nutrients, in the context of marine microbial communities (Keller and Hood, 2013). Viral dynamics in this model assumes that viral decay depends on virus density squared, rather

than being proportional to virus density. A higher-order leading term for viral decay is not part of standard models of virus–host population dyanamics (Levin *et al.*, 1977; Thingstad and Lignell, 1997; Thingstad, 2000; Beretta and Kuang, 2001; Beretta *et al.*, 2002; Weitz *et al.*, 2005; Menge and Weitz, 2009). Moreover, the number of infective viral particles in culture have been shown to decay exponentially, consistent with decay being a first-order process such that the population-level decay rate is proportional to virus density (De Paepe and Taddei, 2006). This difference may have unintended consequences on system dynamics. However, given the complexity of the remainder of the model in Keller and Hood (2013) (treating the microbial ecosystem with greater realism than considered here) steady-state derivations were not possible, limiting the ability to infer the effect of this choice on model dynamics without extensive numerical analysis. On the other hand, it is unlikely that purely exponential decay of viruses and type-I interactions with host populations (as we proposed) is to be expected. For example, marine viruses can be the target of grazing (Gonzalez and Suttle, 1993), adsorb to and aggregate on larger particles, such as marine snow (Weinbauer *et al.*, 2009), and their life history traits, for example, replication rates (Lindell *et al.*, 2007), burst sizes (Wilson *et al.*, 1996) and latent periods (Baudoux *et al.*, 2012), also depend on the physiological status of hosts. All of these factors would potentially give rise to higher-order loss terms or deviations from models with strict type-I functional responses (for example, see Weitz and Dushoff, 2008). Such higher-order losses have the potential to further shift the system away from top-down control by viruses.

In closing, the extension of NPHZ models to include a viral class and explicit nutrient dynamics highlights the potential effects that viruses have within multitrophic communities. Our choice in selecting a relatively low-complexity model representation enabled us to evaluate whether or not long-standing hypotheses regarding the stimulating nature of the viral shunt are consistent with dynamic nutrient feedbacks and their quantitative parameterization. We found that although viruses can have deleterious effects to the hosts they infect and lyse, they may nonetheless have a stimulatory effect at population and ecosystem scales. The dynamics emerging from the model also suggest that introduction of viruses that recycle nutrients can lead to ecosystem effects that are on a continuum between archetypal predictions of bottom-up and top-down control. It is our hope that the current model helps to identify the current state of uncertainty with respect to both the qualitative nature of virus–host interactions and the quantitative rates at which such interactions occur. In the process, we are also hopeful that the present NPHZ-V model provides a motivation for the critical need to collect quantitative data on virus–host interactions in marine surface waters so as to meaningfully integrate viral pools into predictive, global Earth system models.

Conflict of Interest

The authors declare no conflict of interest.

Acknowledgements

This work was supported by participation in the Ocean Viral Dynamics working group at the National Institute for Mathematical and Biological Synthesis, an Institute sponsored by the National Science Foundation, the US Department of Homeland Security and the US Department of Agriculture through NSF Award EF-0832858, with additional support from The University of Tennessee, Knoxville. JSW acknowledges support from a Career Award at the Scientific Interface from the Burroughs Wellcome Fund and NSF OCE-1233760. We thank J Brum and M Sullivan for helpful comments on the manuscript.

References

Allen LZ, Ishoey T, Novotny MA, McLean JS, Lasken RS, Williamson SJ. (2011). Single virus genomics: a new tool for virus discovery. *PLoS One* **6**: e17722.

Ankrah NYD, May AL, Middleton JL, Jones DR, Hadden MK, Gooding JR *et al.* (2014). Phage infection of an environmentally relevant marine bacterium alters host metabolism and lysate composition *ISME J* **8**: 1089–1100.

Armstrong RA, McGehee R. (1980). Competitive exclusion. *Am Nat* **115**: 151–170.

Barber RT, Marra J, Bidigare RC, Codispoti LA, Halpern D, Johnson Z *et al.* (2001). Primary productivity and its regulation in the Arabian Sea during 1995. *Deep Sea Res Part II:* Top Stud Oceanogr **48**: 1127–1172.

Baudoux A-C, Hendrix RW, Lander GC, Bailly X, Podell S, Paillard C *et al.* (2012). Genomic and functional analysis of *Vibrio* phage SIO-2 reveals novel insights into ecology and evolution of marine siphoviruses. *Environ Microbiol* **14**: 2071–2086.

Beretta E, Kuang Y. (2001). Modeling and analysis of a marine bacteriophage infection with latency period. *Nonl Anal* **2**: 35–74.

Beretta E, Solimano F, Tang Y. (2002). Analysis of a chemostat model for bacteria and virulent bacteriophage. *Discrete Continuous Dyn Syst* **2**: 495–520.

Bidle KD, Vardi A. (2011). A chemical arms race at sea mediates algal host-virus interactions. *Curr Opin Microbiol* **14**: 449–457.

Bonachela JA, Levin SA. (2014). Evolutionary comparison between viral lysis rate and latent period. *J Theor Biol* **345**: 32–42.

Bratbak G, Heldal M, Thingstad TF, Riemann B, Haslund OH. (1992). Incorporation of viruses into the budget of microbial C-transfer: a first approach. *Mar Ecol Prog Ser* **83**: 273–280.

Breitbart M. (2012). Marine viruses: truth or dare. *Annu Rev Mar Sci* **4**: 425–448.

Breitbart M, Salamon P, Andresen B, Mahaffy JM, Segall AM, Mead D *et al.* (2002). Genomic analysis

of uncultured marine viral communities. *Proc Natl Acad Sci USA* **99**: 14250–14255.
Brussaard CPD, Wilhelm SW, Thingstad F, Weinbauer MG, Bratbak G, Heldal M *et al.* (2008). Global-scale processes with a nanoscale drive: the role of marine viruses. *ISME J* **2**: 575–578.
Carpenter SR, Kitchell JF, Hodgson JR. (1985). Cascading trophic interactions and lake productivity. *BioSci* **35**: 634–639.
Corinaldesi C, Dell'Anno A, Magagnini M, Danovaro R. (2010). Viral decay and viral production rates in continental-shelf and deep-sea sediments of the Mediterranean Sea. *FEMS Microbiol Ecol* **72**: 208–218.
Danovaro R, Corinaldesi C, Dell'Anno A, Fuhrman JA, Middelburg JJ, Noble RT *et al.* (2011). Marine viruses and global climate change. *FEMS Microbiol Rev* **35**: 993–1034.
De Paepe M, Taddei F. (2006). Viruses' life history: towards a mechanistic basis of a trade-off between survival and reproduction among phages. *PLoS Biol* **4**: e193.
Deng L, Gregory A, Yilmaz S, Poulos BT, Hugenholtz P, Sullivan MB. (2012). Contrasting life strategies of viruses that infect photo- and heterotrophic bacteria, as revealed by viral tagging. *mBio* **3**: e00373–12.
Dunne JA, Laferty KD, Dobson AP, Hechinger RF, Kuris AM, Martinez ND *et al.* (2013). Parasites affect food web structure primarily through increased diversity and complexity. *PLoS Biol* **11**: e1001579.
Edwards RA, Rohwer F. (2005). Viral metagenomics. *Nat Rev Microb* **3**: 504–510.
Flores CO, Meyer JR, Valverde S, Farr L, Weitz JS. (2011). Statistical structure of host-phage interactions. *Proc Natl Acad Sci USA* **108**: E288–E297.
Follows MJ, Dutkiewicz S, Grant S, Chisholm SW. (2007). Emergent biogeography of microbial communities in a model ocean. *Science* **315**: 1843–1846.
Fuhrman JA. (1999). Marine viruses and their biogeochemical and ecological effects. *Nature* **399**: 541–548.
Fuhrman JA, Noble RT. (1995). Viruses and protists cause similar bacterial mortality in coastal seawater. *Limnol Oceanogr* **40**: 1236–1242.
Gobler CJ, Hutchins DA, Fisher NS, Cosper EM, Sañudo-Wilhelmy SA. (1997). Release and bioavailability of C, N, P, Se, and Fe following viral lysis of a marine chrysophyte. *Limnol Oceanogr* **42**: 1492–1504.
Gonzalez JM, Suttle CA. (1993). Grazing by marine nanoflagellates on viruses and virus–sized particles: ingestion and digestion. *Mar Ecol Prog Ser* **94**: 1–10.
Gutenkunst RN, Waterfall JJ, Casey FP, Brown KS, Myers CR, Sethna JP. (2007). Universally sloppy parameter sensitivities in systems biology models. *PLoS Comput Biol* **3**: 1871–1878.
Heath MR, Speirs DC, Steele JH. (2014). Understanding patterns and processes in models of trophic cascades. *Ecol Lett* **17**: 101–114.
Hunter MD, Price PW. (1992). Playing chutes and ladders: heterogeneity and the relative roles of bottom-up and top-down forces in natural communities. *Ecology* **73**: 724–732.
Jacobsen A, Bratbak G, Heldal M. (1996). Isolation and characterization of a virus infecting *Phaeocystis pouchetii* (prymnesiophyceae). *J Phycol* **32**: 923–927.
Johnson ZI, Zinser ER, Coe A, McNulty NP, Woodward EMS, Chisholm SW. (2006). Niche partitioning among *Prochlorococcus* ecotypes along ocean-scale environmental gradients. *Science* **311**: 1737–1740.
Jover LF, Effler TC, Buchan A, Wilhelm SW, Weitz JS. (2014). The elemental composition of virus particles: implications for marine biogeochemical cycles. *Nat Rev Microbiol* **12**: 519–528.
Keller DP, Hood RR. (2013). Comparative simulations of dissolved organic matter cycling in idealized oceanic, coastal, and estuarine surface waters. *J Mar Syst* **109-110**: 109–128.
Klausmeier CA, Litchman E, Levin SA. (2004). Phytoplankton growth and stoichiometry under multiple nutrient limitation. *Limnol Oceanogr* **49**: 1463–1470.
Laferty KD, Allesina S, Arim M, Briggs CJ, De Leo G, Dobson AP *et al.* (2008). Parasites in food webs: the ultimate missing links. *Ecol Lett* **11**: 533–546.
Legovic T, Cruzado A. (1997). A model of phytoplankton growth on multiple nutrients based on the Michaelis-Menten-Monod uptake, Droop's growth and Liebig's law. *Ecol Model* **99**: 19–31.
Letscher RT, Hansell DA, Carlson CA, Lumpkin R, Knapp AN. (2013). Dissolved organic nitrogen in the global surface ocean: distribution and fate. *Global Biogeochem Cycles* **27**: 141–153.
Levin BR, Stewart FM, Chao L. (1977). Resource-limited growth, competition, and predation: a model and experimental studies with bacteria and bacteriophage. *Am Nat* **111**: 3–24.
Lindell D, Jaffe JD, Coleman ML, Futschik ME, Axmann IM, Rector T *et al.* (2007). Genome-wide expression dynamics of a marine virus and host reveal features of co-evolution. *Nature* **449**: 83–86.
Lomas MW, Moran SB. (2011). Evidence for aggregation and export of cyanobacteria and nano-eukaryotes from the Sargasso Sea euphotic zone. *Biogeosciences* **8**: 203–216.
Martiny AC, Pham CTA, Primeau FW, Vrugt JA, Moore JK, Levin SA *et al.* (2013). Strong latitudinal patterns in the elemental ratios of marine plankton and organic matter. *Nat Geosci* **6**: 279–283.
McDaniel L, Breitbart M, Mobberley J, Long A, Haynes M, Rohwer F *et al.* (2008). Metagenomic analysis of lysogeny in Tampa Bay: implications for prophage gene expression. *PLoS One* **3**: e3263.
McKay MD, Beckman RJ, Conover WJ. (1979). A comparison of three methods for selecting values of input variables in the analysis of output from a computer code. *Technometrics* **21**: 239–245.
Menge DNL, Weitz JS. (2009). Dangerous nutrients: evolution of phytoplankton resource uptake subject to virus attack. *J Theor Biol* **257**: 104–115.
Middelboe M, Glud RN. (2006). Viral activity along a trophic gradient in continental margin sediments off central Chile. *Mar Biol Res* **2**: 41–51.
Middelboe M, Jorgensen NOG, Kroer N. (1996). Effects of viruses on nutrient turnover and growth efficiency of noninfected marine bacterioplankton. *Appl Environ Microbiol* **62**: 1991–1997.
Middelboe M, Riemann L, Steward GF, Hansen V, Nybroe O. (2003). Virus-induced transfer of organic carbon between marine bacteria in a model community. *Aquat Microbial Ecol* **33**: 1–10.
Miki T, Nakazawa T, Yokokawa T, Nagata T. (2008). Functional consequences of viral impacts on bacterial communities: a food-web model analysis. *Freshwater Biol* **53**: 1142–1153.
Murray AG, Jackson GA. (1992). Viral dynamics: a model of the effects of size, shape, motion and abundance of single-celled planktonic organisms and other particles. *Mar Ecol Prog Ser* **89**: 103–116.

Pace MG, Cole JF, Carpenter SR, Kitchell JJ. (1999). Trophic cascades revealed in diverse ecosystems. *Trends Ecol Evol* **14**: 483–488.
Poorvin L, Rinta-Kanto JM, Hutchins DA, Wilhelm SW. (2004). Viral release of iron and its bioavailability to marine plankton. *Limnol Oceanogr* **49**: 1734–1741.
Raytcheva DA, Haase-Pettingell C, Piret JM, King J. (2011). Intracellular assembly of cyanophage Syn5 proceeds through a scaffold-containing procapsid. *J Virol* **85**: 2406–2415.
Ruardij P, Veldhuis MJW, Brussaard CPD. (2005). Modeling the bloom dynamics of the polymorphic phytoplankter *Phaeocystis globosa*: impact of grazers and viruses. *Harmful Algae* **4**: 941–963.
Schartau M, Landry MR, Armstrong RA. (2010). Density estimation of plankton size spectra: a reanalysis of IronEx II data. *J Plankton Res* **32**: 1167–1184.
Shelford EJ, Middelboe MM, Møller EF, Suttle CAS. (2012). Virus-driven nitrogen cycling enhances phytoplankton growth. *Aquat Microbial Ecol* **66**: 41–46.
Siem-Jorgensen M, Glud RN, Middelboe M. (2008). Viral dynamics in a coastal sediment: seasonal pattern, controlling factors and relations to the pelagic-benthic coupling. *Mar Biol Res* **4**: 165–U20.
Smith HL, Thieme HR. (2012). Persistence of bacteria and phages in a chemostat. *J Math Biol* **64**: 951–979.
Sterner RW, Elser JJ. (2002). *Ecological Stoichiometry: the Biology of Elements from Molecules to the Biosphere*. Princeton University Press: Princeton, NJ.
Stock CA, Dunne JP, John JG. (2014). Global-scale carbon and energy flows through the marine planktonic food web: an analysis with a coupled physical-biological model. *Prog Oceanogr* **120**: 1–28.
Strogatz SH. (1994). *Nonlinear Dynamics and Chaos*. Addison Wesley: Reading, MA.
Suttle CA. (1994). The significance of viruses to mortality in aquatic microbial communities. *Microb Ecol* **28**: 237–243.
Suttle CA. (2005). Viruses in the sea. *Nature* **437**: 356–361.
Suttle CA. (2007). Marine viruses - major players in the global ecosystem. *Nat Rev Microbiol* **5**: 801–812.
Suttle CA, Chan AM. (1993). Marine cyanophages infecting oceanic and coastal strains of Synechococcus: abundance, morphology, cross-infectivity and growth characteristics. *Mar Ecol Prog Ser* **92**: 99–109.
Thingstad TF. (2000). Elements of a theory for the mechanisms controlling abundance, diversity, and biogeochemical role of lytic bacterial viruses in aquatic systems. *Limnol Oceanogr* **45**: 1320–1328.
Thingstad TF, Lignell R. (1997). Theoretical models for the control of bacterial growth rate, abundance, diversity and carbon demand. *Aquat Microb Ecol* **13**: 19–27.
Umani SF, Malisana E, Focaracci F, Magagnini M, Corinaldesi C, Danovaro R. (2010). Disentangling the effect of viruses and nanoflagellates on prokaryotes in bathypelagic waters of the Mediterranean Sea. *Mar Ecol Prog Ser* **418**: 73–85.
Weinbauer MG, Brettar I, Hofle ML. (2003). Lysogeny and virus-induced mortality of bacterioplankton in surface, deep, and anoxic marine waters. *Limnol Oceanogr* **48**: 1457–1465.
Weinbauer MG. (2004). Ecology of prokaryotic viruses. *FEMS Microbiol Rev* **28**: 127–181.
Weinbauer MG, Bettarel Y, Cattaneo R, Luef B, Maier C, Motegi C *et al.* (2009). Viral ecology of organic and inorganic particles in aquatic systems: avenues for further research. *Aquat Microb Ecol* **57**: 321–341.
Weinbauer MG, Chen F, Wilhelm SW. (2011). Virus-mediated redistribution and partitioning of carbon in the global oceans. In Jiao N, Azam F, Sanders S (eds) *Microbial Carbon Pump in the Ocean*. Science/AAAS: Washington, DC, pp 54–56.
Weitz JS, Dushoff J. (2008). Alternative stable states in host-phage dynamics. *Theor Ecol* **1**: 13–19.
Weitz JS, Hartman H, Levin SA. (2005). Coevolutionary arms races between bacteria and bacteriophage. *Proc Natl Acad Sci USA* **102**: 9535–9540.
Weitz JS, Poisot T, Meyer JR, Flores CO, Valverde S, Sullivan MB *et al.* (2013). Phage-bacteria infection networks. *Trends Microbiol* **21**: 82–91.
Weitz JS, Wilhelm SW. (2012). Ocean viruses and their effects on microbial communities and biogeochemical cycles. *F1000 Biol Rep* **4**: 17.
Wilhelm SW, Matteson AR. (2008). Freshwater and marine virioplankton: a brief overview of commonalities and differences. *Freshw Biol* **53**: 1076–1089.
Wilhelm SW, Suttle CA. (1999). Viruses and nutrient cycles in the sea. *BioScience* **49**: 781–788.
Williams RG, Follows MJ. (2011). *Ocean Dynamics and the Carbon Cycle: Principles and Mechanisms*. Cambridge University Press: Cambridge, UK.
Wilson WH, Carr NG, Mann NH. (1996). The effect of phosphate status on the kinetics of cyanophage infection in the oceanic cyanobacterium *Synechococcus* sp. WH7803. *J Phycol* **32**: 506–516.
Wommack KE, Colwell RR. (2000). Virioplankton: viruses in aquatic ecosystems. *Microbiol Mol Biol Rev* **64**: 69–114.

Supplementary Information accompanies this paper on The ISME Journal website (http://www.nature.com/ismej)

Supplementary Information:

A multitrophic model to quantify the effects of marine viruses on microbial food webs and ecosystem processes

Joshua S. Weitz[1], School of Biology and Physics, Georgia Institute of Technology, Atlanta, GA, USA, **Charles A. Stock**, Geophysical Fluid Dynamics Laboratory, NOAA, Princeton, NJ, USA, **Steven W. Wilhelm**, Department of Microbiology, University of Tennessee, Knoxville, TN, USA, **Lydia Bourouiba**, Department of Applied Mathematics, Massachusetts Institute of Technology, Cambridge, MA, USA, **Alison Buchan**, Department of Microbiology, University of Tennessee, Knoxville, TN, USA, **Maureen L. Coleman**, Department of Geosciences, University of Chicago, Chicago, IL, USA, **Michael J. Follows**, Department of Earth, Atmospheric and Planetary Sciences, Massachusetts Institute of Technology, Cambridge, MA, USA, **Jed A. Fuhrman**, Department of Biological Sciences,University of Southern California, Los Angeles, CA, USA, **Luis F. Jover**, School of Physics, Georgia Institute of Technology, Atlanta, GA, USA, **Jay T. Lennon**, Department of Biology, Indiana University, Bloomington, IN, USA, **Mathias Middelboe**, Marine Biological Section, University of Copenhagen, Copenhagen, Denmark, **Derek L. Sonderegger**, Department of Mathematics, Northern Arizona University, Flagstaff, AZ, USA, **Curtis A. Suttle**, Department of Earth and Ocean Sciences, Department of Botany and Department of Immunology and Microbiology, University of British Columbia, Vancouver, British Columbia, Canada, **Bradford P. Taylor**, School of Physics, Georgia Institute of Technology, Atlanta, GA, USA, **T. Frede Thingstad**, Department of Biology, University of Bergen, Bergen, Norway, **William H. Wilson**, Bigelow Laboratory for Ocean Sciences, East Boothbay, ME, USA; current address: Plymouth Marine Laboratory, Plymouth, UK and **K. Eric Wommack**, Delaware Biotechnology Institute, University of Delaware, Newark, DE, USA

1 NPHZ-V model of microbial ecosystem dynamics

1.1 Model with viruses

We propose the following systems of equations to represent the dynamic changes of biotic populations, including heterotrophs (H), cynanobacteria (C), eukaryotic autotrophs (E), zooplankton (Z) and viruses (V_i where $i = H, C$, and E), along with organic and inorganic nutrients (x_{on} and x_{in} respectively). The system of equations (S1-S9) are nonlinear, coupled ODEs. Eq. (S10) makes explicit the export from the system to higher trophic levels. We use units of particles/L for all populations and μmol/L for nutrient concentrations. Hence, conversion factors, q, denote the equivalent nitrogen content of cells. Definition of parameters are in Table S1. Parameters include those associated with interactions and with the nutrient content of each biotic population on a per-cell basis.

[1]Email: jsweitz@gatech.edu

$$\text{Heterotrophs: } \dot{H} = \overbrace{\frac{\mu_H H x_{on}}{x_{on}+K_{on}}}^{\text{H growth}} - \overbrace{\phi_{VH} H V_H}^{\text{viral lysis}} - \overbrace{\psi_{ZH} H Z}^{\text{grazing}} - \overbrace{m_{on,H} H}^{\text{organic loss}} - \overbrace{m_{in,H} H}^{\text{respiration}} \tag{S1}$$

$$\text{Cyanobacteria: } \dot{C} = \overbrace{\frac{\mu_C C x_{in}}{x_{in}+K_{in,C}}}^{\text{C growth}} - \overbrace{\phi_{VC} C V_C}^{\text{viral lysis}} - \overbrace{\psi_{ZC} C Z}^{\text{grazing}} - \overbrace{m_{on,C} C}^{\text{organic loss}} - \overbrace{m_{in,C} C}^{\text{respiration}} \tag{S2}$$

$$\text{Euk. autos: } \dot{E} = \overbrace{\frac{\mu_E E x_{in}}{x_{in}+K_{in,E}}}^{\text{E growth}} - \overbrace{\phi_{VE} E V_E}^{\text{viral lysis}} - \overbrace{\psi_{ZE} E Z}^{\text{grazing}} - \overbrace{m_{on,E} E}^{\text{organic loss}} - \overbrace{m_{in,E} E}^{\text{respiration}} \tag{S3}$$

$$\text{Zooplankton } \dot{Z} = \overbrace{p_g\left(\frac{q_H}{q_Z}\psi_{ZH} H Z + \frac{q_C}{q_Z}\psi_{ZC} C Z + \frac{q_E}{q_Z}\psi_{ZE} E Z\right)}^{\text{grazing}} - \overbrace{m_Z Z}^{\text{respiration}} - \overbrace{m_{ZP} Z^2}^{\text{consumption}} \tag{S4}$$

$$\text{Viruses of H: } \dot{V_H} = \overbrace{\beta_H \phi_{VH} H V_H}^{\text{lysis}} - \overbrace{m_{VH} V_H}^{\text{decay}} \tag{S5}$$

$$\text{Viruses of C: } \dot{V_C} = \overbrace{\beta_C \phi_{VC} C V_C}^{\text{lysis}} - \overbrace{m_{VC} V_C}^{\text{decay}} \tag{S6}$$

$$\text{Viruses of E: } \dot{V_E} = \overbrace{\beta_E \phi_{VE} E V_E}^{\text{lysis}} - \overbrace{m_{VE} V_E}^{\text{decay}} \tag{S7}$$

$$\begin{aligned}\text{Organic N: } \dot{x}_{on} = & -\overbrace{\frac{q_H}{\epsilon_H}\frac{\mu_H H x_{on}}{x_{on}+K_{on}}}^{\text{H growth}} + \overbrace{q_V m_{VH} V_H + q_V m_{VC} V_C + q_V m_{VE} V_E}^{\text{viral decay}} \\ & + \overbrace{(q_H - q_V\beta_H)\phi_{VH} H V_H}^{\text{H lysis by viruses}} + \overbrace{(q_C - q_V\beta_C)\phi_{VC} C V_C}^{\text{C lysis by viruses}} + \overbrace{(q_E - q_V\beta_E)\phi_{VE} E V_E}^{\text{E lysis by viruses}} \\ & + \overbrace{q_H m_{on,H} H}^{\text{loss of H}} + \overbrace{q_C m_{on,C} C}^{\text{loss of E}} + \overbrace{q_E m_{on,E} E}^{\text{loss of C}} \\ & + \overbrace{p_{on} q_H \psi_{ZH} H Z}^{\text{H grazing by Z}} + \overbrace{p_{on} q_C \psi_{ZC} C Z}^{\text{C grazing by Z}} + \overbrace{p_{on} q_E \psi_{ZE} E Z}^{\text{E grazing by Z}}\end{aligned} \tag{S8}$$

$$\begin{aligned}\text{Inorganic N: } \dot{x}_{in} = & \overbrace{-\omega(x_{in} - x_{sub})}^{\text{import}} + \overbrace{\frac{q_H(1-\epsilon_H)}{\epsilon_H}\frac{\mu_H H x_{on}}{x_{on}+K_{on}}}^{\text{H growth}} - \overbrace{\frac{q_C \mu_C C x_{in}}{x_{in}+K_{in,C}}}^{\text{C growth}} - \overbrace{\frac{q_E \mu_E E x_{in}}{x_{in}+K_{in,E}}}^{\text{E growth}} + \overbrace{q_Z m_z Z}^{\text{respiration}} \\ & + \overbrace{q_H m_{in,H} H}^{\text{respiration of H}} + \overbrace{q_C m_{in,C} C}^{\text{respiration of E}} + \overbrace{q_E m_{in,E} E}^{\text{respiration of C}} \\ & + \overbrace{p_{in} q_H \psi_{ZH} H Z}^{\text{H grazing by Z}} + \overbrace{p_{in} q_C \psi_{ZC} C Z}^{\text{C grazing by Z}} + \overbrace{p_{in} q_E \psi_{ZE} E Z}^{\text{E grazing by Z}}\end{aligned} \tag{S9}$$

$$\text{Export : } J_{out} = \overbrace{p_{ex} q_Z m_{ZP} Z^2}^{\text{consumption}} \tag{S10}$$

1.2 Model without viruses

We propose an alternative model without viruses:

$$\text{Heterotrophs: } \dot{H} = \overbrace{\frac{\mu_H H x_{on}}{x_{on}+K_{on}}}^{\text{H growth}} - \overbrace{\psi_{ZH}HZ}^{\text{grazing}} - \overbrace{m_{on,H}H}^{\text{organic loss}} - \overbrace{m_{in,H}H}^{\text{respiration}} \tag{S11}$$

$$\text{Cyanobacteria: } \dot{C} = \overbrace{\frac{\mu_C C x_{in}}{x_{in}+K_{in,C}}}^{\text{C growth}} - \overbrace{\psi_{ZC}CZ}^{\text{grazing}} - \overbrace{m_{on,C}C}^{\text{organic loss}} - \overbrace{m_{in,C}C}^{\text{respiration}} \tag{S12}$$

$$\text{Euk. autos: } \dot{E} = \overbrace{\frac{\mu_E E x_{in}}{x_{in}+K_{in,E}}}^{\text{E growth}} - \overbrace{\psi_{ZE}EZ}^{\text{grazing}} - \overbrace{m_{on,E}E}^{\text{organic loss}} - \overbrace{m_{in,E}E}^{\text{respiration}} \tag{S13}$$

$$\text{Zooplankton } \dot{Z} = \overbrace{p_g\left(\frac{q_H}{q_Z}\psi_{ZH}HZ + \frac{q_C}{q_Z}\psi_{ZC}CZ + \frac{q_E}{q_Z}\psi_{ZE}EZ\right)}^{\text{grazing}} - \overbrace{m_Z Z}^{\text{respiration}} - \overbrace{m_{ZP}Z^2}^{\text{consumption}} \tag{S14}$$

$$\begin{aligned}\text{Organic N: } \dot{x}_{on} = & -\overbrace{\frac{q_H}{\epsilon_H}\frac{\mu_H H x_{on}}{x_{on}+K_{on}}}^{\text{H growth}} + \overbrace{q_H m_{on,H}H}^{\text{loss of H}} + \overbrace{q_C m_{on,C}C}^{\text{loss of E}} + \overbrace{q_E m_{on,E}E}^{\text{loss of C}} \\ & + \overbrace{p_{on}q_H\psi_{ZH}HZ}^{\text{H grazing by Z}} + \overbrace{p_{on}q_C\psi_{ZC}CZ}^{\text{C grazing by Z}} + \overbrace{p_{on}q_E\psi_{ZE}EZ}^{\text{E grazing by Z}}\end{aligned} \tag{S15}$$

$$\begin{aligned}\text{Inorganic N: } \dot{x}_{in} = & \overbrace{-\omega(x_{in}-x_{sub})}^{\text{import}} + \overbrace{\frac{q_H(1-\epsilon_H)}{\epsilon_H}\frac{\mu_H H x_{on}}{x_{on}+K_{on}}}^{\text{H growth}} - \overbrace{\frac{q_C\mu_C C x_{in}}{x_{in}+K_{in,C}}}^{\text{C growth}} - \overbrace{\frac{q_E\mu_E E x_{in}}{x_{in}+K_{in,E}}}^{\text{E growth}} + \overbrace{q_Z m_z Z}^{\text{respiration}} \\ & + \overbrace{p_{in}q_H\psi_{ZH}HZ}^{\text{H grazing by Z}} + \overbrace{p_{in}q_C\psi_{ZC}CZ}^{\text{C grazing by Z}} + \overbrace{p_{in}q_E\psi_{ZE}EZ}^{\text{E grazing by Z}} \\ & + \overbrace{q_H m_{in,H}H}^{\text{respiration of H}} + \overbrace{q_C m_{in,C}C}^{\text{respiration of E}} + \overbrace{q_E m_{in,E}E}^{\text{respiration of C}}\end{aligned} \tag{S16}$$

$$\text{Export : } J_{out} = \overbrace{p_{ex}q_Z m_{ZP}Z^2}^{\text{consumption}} \tag{S17}$$

1.3 Simulation framework

All simulations are conducted in MATLAB. The two models, with and without viruses, are simulated using the same codebase. The code accepts a set of interactions and then builds a coupled system of ODE-s out of this set. Numerical integration of the coupled system of ODE-s is done using a higher order Runga-Kutta integration scheme (ode45 in MATLAB). A complete README is available and the source code is available for use without restriction as a Supplementary File and is available for download at GitHub.

2 Parameter estimation

2.1 Rationale for upper and lower bounds of model parameters

Initial parameter ranges in Table S2 were based on established values in models of aquatic food webs with viruses [27, 17] and without viruses [28, 22]. Because the current model differs in structure, some of the parameter variation may have been due to virus effects and not explicitly modeled. As such, we tried, when possible, to select broader potential parameter regimes for model selection, and utilized our targeted parameter search to identify those combinations of parameters that were compatible with biologically plausible concentrations. Below are details on the rationale for parameter range selection, organized by event type.

H growth : Heterotrophs can double on rates that vary from hourly to daily. However, as a functional group, we utilized conventions of μ_H of approximately 0.5 to 2 days^{-1}, consistent estimates ranging from $0.1 - 2$ days^{-1} [7]. The half-saturation constant, K_{on}, are based on estimates of 0.5 μM N cited in [4]. The growth efficiency ϵ_H is based on ranges established in [6] for ocean systems that have the bulk of their variation between 0.1-0.3, with biological variation outside of that range.

C growth : Cyanobacteria doubling times are approximately 12 hrs-24 hrs [29] - which we expand to include rates that correspond to approximately 0.5 to 2 days^{-1}. The half-saturation rates are chosen from the low end of reported phytoplankton ranges, which have been reported to be less than 0.2 μmol/L for natural oceanic communities, to include the range 0.05 to 1 μmol/L [9, 8].

E growth : Eukaryotic autotrophs have maximum growth rates of hours to days, with substantial variation given variation in nutrient availability. Yet, they can also have higher half-saturation constants than do cyanobacteria with estimates of $K_{in,E}$ reaching 10 μmol/L [14, 21, 15]. In practice, we select half-saturation constants in the range of reported values from 0.5 to 10μmol/L [9, 21], and maximum growth rates from 0.2 to 2 days^{-1}.

Viral lysis : Maximum values of diffusion-limited adsorption rates are approximately 2×10^{-9} L/(viruses-days) given a microbial host with 2 μm diameter and a virus with a 50 nm diameter capsid. This rate increases proportionately with host diameter and the inverse of virus effective radius. However, realized diffusion-limited adsorption rates are less for biophysical reasons, e.g., receptors are not uniformly distributed on cell surfaces, and ecological reasons, e.g., not all host cells are targeted by all viruses [18]. Here we set the upper limit of adsorption to be 5 times below the maximum. In practice, we selected a lower range two or three orders of magnitude below. Next, burst sizes vary significantly for viruses of marine microbes. We used baseline estimates that burst sizes range from 20-40 for lysis of marine heterotrophs [20]. We permitted higher upper ranges (up to 100) for infections of cyanobacteria even higher upper ranges (up to 500) for infections of microeukaryotes [3]. Upper limits of lysis in certain infections of large phytoplankton have been reported but were not included in the ranges [3].

Viral decay : Residence times of virus particles in the upper surface ocean have been estimated to be on the order of 1 day [25]. Here we permit potentially faster clearance, at a rate up to 5 days^{-1}. Intrinsic decay rates have been estimated to be on the order of weeks at room temperature [5] which sets our lower limit of decay of 0.05 days^{-1}.

Zooplankton grazing Stock and Dunne [22] implemented a Type-II functional response for grazing. Here, we utilize a Type-I functional response. These can be compared in the limit of small prey densities. Stock and Dunne [22] report:

$$\frac{I_{max,SZ}}{K_{I,SZ}} = \frac{5}{[0.68 - 1.18]} \frac{m^3}{day\, mmoles N} = 4.2 - 7.4 \frac{L}{day\, \mu mol\, N}$$

The range used here is inclusive with:

$$\frac{\psi}{q_Z} = \frac{[10^{-6} - 10^{-4}]}{[5 \times 10^{-5} 4 \times 10^{-4}]} \frac{L}{day\, \mu mol\, N} = 0.025 - 20 \frac{L}{day\, \mu mol\, N}$$

consistent with observations in [12]. The use of an extended lower limit enables the exploration of a dynamic range in which zooplankton are relatively less efficient than viruses in clearing hosts. The value of the half-saturation constant, $K_{I,SZ}$ in [22] was calibrated to their data and does not have an analogous parameter in the current model. The fixed value of 40% assimilation efficiency p_g is based on measurements of approximately 20%-40% efficiency for nano-microflagellates, with additional variation outside of this 75% confidence interval [23]. The breakdown between egestion, p_{on}, and respiration, p_in, are based on outcomes reported in [19].

Grazer respiration Stock and Dunne [22] used ranges: 0.05-0.4 day^{-1} for small zooplankton and 0.02-0.16 day^{-1} for large zooplankton. Here we utilize the range $0.025 - 0.1 day^{-1}$.

Consumption by higher predators The parameter m_{ZP} enables the closure of the model, as it corresponds to consumption of the "top" predator in the current model by other, larger predators. A fraction, p_{ex} of this is transferred out of the system to higher trophic levels. The limits were calibrated to ensure model coexistence in a plausible regime.

Import The concentration of inorganic nutrient below the nutricline determined the value of x_{sub} [28]. The stable mixed layer has a turnover time ranging from 50 to 200 days. This is a feature of the assumption of a highly retentive surface microbial ecosystem as modeled here.

Nutrient levels Cyanobacteria nitrogen content can vary with strain and growth conditions, e.g., from approximately 10 to 50 fg per cell with the strains *Prochlorococcus* MED4, *Synechococcus* WH8012 and *Synechococcus* WH8013 respectively [2]. This range corresponds to 0.7×10^{-9} to 3.5×10^{-9} μmol N per cell, which is used as the basis for the selected range of $0.5\text{-}4\times10^{-9}$. Note that although heterotrophic cell sizes can be smaller, e.g., on the order of 20 fg per cell [7], they also differ in the nutrient content, with larger-than-expected nitrogen-to-carbon ratios [24]. Here, an identical range for nitrogen content is used for heterotrophs. Eukaryotic autotrophs spanning a size range $2-5$ μm in size are approximately 5 times large in size. This increase in physical dimension translates into an approximately two-order of magnitude increase in carbon and nitrogen content, such that we assume $q_E \approx 2\times10^{-7}$ μmol N/cell and include variation around this baseline. The nano-/micro-zooplankton group are assumed to be 1 order of magnitude larger in physical dimension, i.e., between $10-50$ μ m in size, such that they have a baseline nitrogen content of $q_Z \approx 10^{-4}$ μmol N/cell with variation around that value. Finally, viral nitrogen content, q_V, has been estimated via a first principles biophysical theory to range between $1.4\times10^{-12}-14\times10^{-12}$ μmol N/(virus particle) for viruses whose capsids have diameters between 30-70 nm [13]. Estimates for nutrient content of viruses are based on estimates focusing on the heads of bacteriophage particles containing dsDNA without lipids. We expand this range to account for potential biological variation, in both size and structure, across all three types, ranging from 0.5×10^{-12} to 20×10^{-12} μmol N/particle.

Cellular loss We include a linear loss of phytoplankton to inorganic material to represent basal metabolic losses and a similar loss to organic material to represent exudation. Basal respiration ranges were informed by baseline estimates of 10% relative to production rates, using 1 per day production as a baseline [10] (while noting that variation can be substantial, particular during starvation periods). Basal exudation rates were informed by [1], which estimates that approximately 13% of total fixed organic matter is released. We set the upper range to be approximately 1/10 of maximum growth rates when growing at a rate of 1 per day. The model analysis is robust to choices in these ranges, so long as dominant forms of mortality are due to interactions rather than death due to loss of viability in the absence of nutrients (i.e., exudation and respiration).

2.2 Constraints on parameter combinations

Parameters within bounds, delineated above, cannot always be chosen independently. In particular, the nitrogen content of virions released upon lysis cannot exceed the nitrogen content of uninfected hosts. Hence, we find the following self-consistency conditions:

$$q_H > q_V\beta_{VH} \qquad q_C > q_V\beta_{VC} \qquad q_E > q_V\beta_{VE}$$

where β denotes the burst size of a particular viral-host interaction (denoted in the subscript). Similarly, for self-consistency, the nitrogen content of zooplankton produced due to grazing cannot exceed the nitrogen content of hosts consumed. This is ensured by using ratios of the species q-values multiplied by a fractional use. Note that the ultimate destination of organic material grazed by zooplankton must satisfy:

$$\overbrace{p_g}^{\text{growth}} + \overbrace{p_{on}}^{\text{egestion}} + \overbrace{p_{in}}^{\text{respiration}} = 1$$

Finally, at steady state export must balance import, which reflects the balance of net import of inorganic N with the export of organic N (either up the food chain or exported out of the surface layer).

3 Analytical solutions of the coexistence steady state in models with and without viruses

3.1 Algebraic solutions of the steady state for the model with viruses

The derivation of steady states is the multi-trophic model with viruses is straightforward, though not all of the algebraic solutions yield significant insight. For completeness, we present the derivation in its entirety. To begin, set equations (5-7) to 0, yielding:

$$H^* = \frac{m_{VH}}{\beta_H \phi_{VH}} \tag{S18}$$

$$C^* = \frac{m_{VC}}{\beta_C \phi_{VC}} \tag{S19}$$

$$E^* = \frac{m_{VE}}{\beta_E \phi_{VE}} \tag{S20}$$

where the asterisks denote steady state densities. Further, note that grazer dynamics only depend on Z and the densities of the three microbial guilds. Hence, Z^* can also be solved:

$$Z^* = \frac{\frac{p_g}{q_Z}\left(q_H \psi_{ZH} H^* + q_C \psi_{ZC} C^* + q_E \psi_{ZE} E^*\right) - m_Z}{m_{ZP}} \tag{S21}$$

Because of nutrient balance, we also have a solution for x_{in}^*:

$$x_{in}^* = x_{sub} - \frac{q_Z m_{ZP} \left(Z^*\right)^2}{\omega} \tag{S22}$$

With this in hand, we also have solutions for the viral levels of cyanobacteria and eukaryotes:

$$V_C^* = \frac{\frac{\mu_C x_{in}^*}{x_{in}^* + K_{in,C}} - \psi_{ZC} Z^* - m_{in,C} - m_{on,C}}{\phi_{VC}} \tag{S23}$$

$$V_E^* = \frac{\frac{\mu_E x_{in}^*}{x_{in}^* + K_{in,E}} - \psi_{ZE} Z^* - m_{in,E} - m_{on,E}}{\phi_{VE}} \tag{S24}$$

Finally, there are two equations that we can use to help solve for x_{on}^* and V_H^*. First, from the dynamics of heterotrophs (Equation 1):

$$\frac{\mu_H x_{on}^*}{x_{on}^* + K_{on}} = \phi_{VH} V_H^* + \psi_{ZH} Z^* + m_{in,H} + m_{on,H} \tag{S25}$$

This implies that:

$$x_{on}^* = \frac{K_{on}\left(\phi_{VH} V_H^* + \psi_{ZH} Z^* + m_{in,H} + m_{on,H}\right)}{\mu_H - \phi_{VH} V_H^* - \psi_{ZH} Z^* - m_{in,H} - m_{on,H}} \tag{S26}$$

This equation is implicit in V_H^*, which we solve next. Then, recalling the dynamics of organic N:

$$\begin{aligned}
\text{Organic N: } \dot{x}_{on} = & -\overbrace{\frac{q_H}{\epsilon_H}\frac{\mu_H H x_{on}}{x_{on} + K_{on}}}^{\text{H growth}} + \overbrace{q_V m_{VH} V_H + q_V m_{VC} V_C + q_V m_{VE} V_E}^{\text{viral decay}} \\
& + \overbrace{(q_H - q_V \beta_H)\phi_{VH} H V_H}^{\text{H lysis by viruses}} + \overbrace{(q_C - q_V \beta_C)\phi_{VC} C V_C}^{\text{C lysis by viruses}} + \overbrace{(q_E - q_V \beta_E)\phi_{VE} E V_E}^{\text{E lysis by viruses}} \\
& + \overbrace{q_H m_{on,H} H}^{\text{loss of H}} + \overbrace{q_C m_{on,C} C}^{\text{loss of E}} + \overbrace{q_E m_{on,E} E}^{\text{loss of C}} \\
& + \overbrace{p_{on} q_H \psi_{ZH} H Z}^{\text{H grazing by Z}} + \overbrace{p_{on} q_C \psi_{ZC} C Z}^{\text{C grazing by Z}} + \overbrace{p_{on} q_E \psi_{ZE} E Z}^{\text{E grazing by Z}}
\end{aligned} \tag{S27}$$

we replace the first term and isolate V_H^* (ignoring the * for now, but we will re-insert them later):

$$\begin{aligned} V_H\left(\frac{q_H\phi_{VH}H}{\epsilon_H} - q_V m_{VH} - (q_H - q_V\beta_H)\phi_{VH}H\right) &= -\frac{q_H H}{\epsilon_H}\left(\psi_{ZH}Z + m_{in,H} + m_{on,H}\right) + q_V m_{VC}V_C + q_V m_{VE}V_E \\ &\quad +(q_C - q_V\beta_C)\phi_{VC}CV_C + (q_E - q_V\beta_E)\phi_{VE}EV_E \\ &\quad +p_{on}q_H\psi_{ZH}HZ + p_{on}q_C\psi_{ZC}CZ + p_{on}q_E\psi_{ZE}EZ \\ &\quad +q_H m_{on,H}H + q_C m_{on,C}C + q_E m_{on,E}E \\ &\equiv \aleph \end{aligned} \tag{S28}$$

And so, omitting * on the right hand side given the size of the equation):

$$V_H^* = \frac{\aleph}{\frac{q_H\phi_{VH}H}{\epsilon_H} - q_V m_{VH} - (q_H - q_V\beta_H)\phi_{VH}H} \tag{S29}$$

Our finding of an algebraic solution facilitates rapid evaluation of the dependence of steady state densities on parameters. We do not claim that the algebraic forms, in and of themselves, are necessarily insightful.

3.2 Algebraic solutions of the virus-free steady state

As discussed in the main text, viruses act to enrich for diversity. Without viruses, then either the cyanophage or the eukaryotic phytoplankton go extinct. From a model standpoint, the reason is that both cyanophage and the eukaryotic phytoplankton functional groups compete for the same (single) resource and are subject to the same grazer. If we had used different functional responses or multiple resources then coexistence could be possible, even without viruses. Hence, let us for a moment consider the case where $C^* = 0$ and all the viruses are zero. In that case, and dropping the * for now, we recognize that the steady state solution can be found as follows.

First, because of nutrient balance, we also have a solution for x_{in}:

$$x_{in} = x_{sub} - \frac{q_Z m_{ZP} Z^2}{\omega} \tag{S30}$$

However, because of the conditions implied by $\dot{E} = 0$, then

$$Z = \frac{1}{\psi_{ZE}}\left[\frac{\mu_E x_{in}}{(x_{in} + K_{in,E})} - m_{on,E} - m_{in,E}\right] \tag{S31}$$

which can substitute back to yield (with $m_E \equiv m_{in,E} + m_{on,E}$):

$$x_{in} = x_{sub} - \frac{q_Z m_{ZP}}{\omega\psi_{ZE}^2}\left[\left(\frac{\mu_E x_{in}}{x_{in} + K_{in,E}}\right)^2 - \frac{2m_E\mu_E x_{in}}{x_{in} + K_{in,E}} + m_E^2\right].$$

Noting that $\mathbb{C} = \frac{q_Z m_{ZP}}{\omega\psi_{ZE}^2}$, we can rewrite this as:

$$x_{in} = x_{sub} - \mathbb{C}\left[\left(\frac{\mu_E x_{in}}{x_{in} + K_{in,E}}\right)^2 - \frac{2m_E\mu_E x_{in}}{x_{in} + K_{in,E}} + m_E^2\right].$$

and re-arranging terms yields:

$$x_{in}\left(x_{in} + K_{in,E}\right)^2 = x_{sub}\left(x_{in} + K_{in,E}\right)^2 - \mathbb{C}\mu_E^2 x_{in}^2 + 2\mathbb{C}m_E\mu_E x_{in}\left(x_{in} + K_{in,E}\right) - \mathbb{C}m_E^2\left(x_{in} + K_{in,E}\right)^2. \tag{S32}$$

We then expand this out in like terms such that

$$x_{in}^3 + C_2 x_{in}^2 + C_1 x_{in} + C_0 = 0$$

where

$$C_2 = 2K_{in,E} - x_{sub} + \mathbb{C}\mu_E^2 - 2\mathbb{C}m_E\mu_E + \mathbb{C}m_E^2 \tag{S33}$$

$$C_1 = K_{in,E}^2 - 2x_{sub}K_{in,E} - 2\mathbb{C}m_E\mu_E K_{in,E} + 2\mathbb{C}m_E^2 K_{in,E} \tag{S34}$$

$$C_0 = -x_{sub}K_{in,E}^2 + \mathbb{C}m_E^2 K_{in,E}^2 \tag{S35}$$

We can then solve this cubic algebraically to find x_{in}^*. It is well known that this may admit 1 or 3 real solutions (ignoring degenerate cases). Defining $\Delta = 18C_2C_1C_0 - 4C_2^3C_0 + C_2^2C_1^2 - 4C_1^3 - 27C_0^2$, we note that when $\Delta > 0$ then there will be three real roots and when $\Delta < 0$ there will be one real root. The sign of Δ and the positivity (or not) of roots is examined numerically.

Next, we work progressively to solve the remainder of the steady state values algebraically, implicit given the value of x_{in}^*. First, zooplankton:

$$Z = \left[\frac{\omega\left(x_{sub} - x_{in}\right)}{q_z m_{ZP}}\right]^{1/2} \tag{S36}$$

then using the $\dot{H} = 0$ condition:

$$x_{on} = \frac{K_{on}\left(\psi_{ZH}Z + m_{on,H} + m_{in,H}\right)}{\mu_H - \psi_{ZH}Z - m_{on,H} - m_{in,H}} \tag{S37}$$

then using the $\dot{x}_{on}$ equation and the relationship implied by the $\dot{Z}$ equation, yields:

$$\begin{aligned} H\left[\frac{q_H\mu_H x_{on}}{\epsilon_H\left(x_{on} + K_{on}\right)} - q_H m_{on,H} + q_E m_{on,E}\frac{q_H\psi_{ZH}}{q_E\psi_{ZE}}\right] &= \frac{p_{on}q_Z Z\left(m_Z + m_{ZP}Z\right)}{p_g} \\ &\quad + q_E m_{on,E}\frac{q_Z\left(m_Z + m_{ZP}Z\right)}{p_g q_E\psi_{ZE}} \end{aligned} \tag{S38}$$

such that

$$H = \frac{\frac{p_{on}q_Z Z(m_Z+m_{ZP}Z)}{p_g} + q_E m_{on,E}\frac{q_Z(m_Z+m_{ZP}Z)}{p_g q_E\psi_{ZE}}}{\left[\frac{q_H\mu_H x_{on}}{\epsilon_H(x_{on}+K_{on})} - q_H m_{on,H} + q_E m_{on,E}\frac{q_H\psi_{ZH}}{q_E\psi_{ZE}}\right]} \tag{S39}$$

and finally,

$$E = \left(m_{ZP}Z + m_Z - p_g q_H\psi_{ZH}H/q_Z\right)\frac{q_Z}{p_g q_E\psi_{ZE}} \tag{S40}$$

Due to the symmetry of the model construction, a similar steady state is found in cases where $E \to 0$ and, instead $C^* > 0$.

3.3 Stability of equilibria

We evaluated the expected stability of feasible fixed points. The stability was evaluated by calculating the Jacobian at the equilibrium. An analytic expression for the Jacobian was evaluated automatically based on the first derivatives of the predicted steady states. The Jacobian was then evaluated given parameters and predicted densities for each fixed point (complete expressions available as a source file in the software release). The stability of the steady state was classified into stable nodes, stable spirals, unstable nodes and unstable spirals. The conditions for each were based on the real and imaginary components of the largest eigenvalue. Stability was determined based on whether the largest eigenvalue was negative (stable) or positive (unstable). Nodes had no imaginary component where spirals did. For example, a fixed point was considered to be a stable spiral if the real part of the largest eigenvalue was negative, but at least one eigenvalue had a non-zero imaginary term.

4 Sensitivity analysis

4.1 Latin-hypercube sampling of parameters

A LHS approach was used to sample parameter space [16]. Of the 38 parameters, 35 were allowed to vary. The three that remained fixed for all models were related to the fractional allocation of prey biomass consumed by zooplankton, i.e., p_g, p_{on}, and p_{in}. We used uniform distributions in logarithmic space where the lower and upper bounds for all parameters are shown in Table S1. We used 10 resamples for each of 10^5 independent selection of midpoints within the stratified 35-dimensional parameter space, for a total of 10^6 random parameter sets.

4.2 Identifying baseline parameters consistent with "known" system densities

Initial parameters were chosen by first establishing approximate values for all parameters from the literature and from first-principle derivations. Given that parameters represent functional groups, these initial values were used to seed an automatic approach to finding parameter sets compatible with steady state densities commonly observed in the surface oceans. Because there are 38 parameters and multiple constraints among parameters, the following automated procedure was developed:

1. An initial guess for all parameters was chosen, denoted as x_0. This value was selected via LHS approach (see Table S2).

2. Lower and upper bounds were selected for all parameters, denoted as x_l and x_h, respectively. The bounds were in most cases a factor of 2 below and above the initial guesses, except for interaction rates which are often most uncertain, which were allowed to vary by 3 or 4 orders of magnitude.

3. A nonlinear minimization routine (fmincon in MATLAB) was utilized to find an optimal set of 38 parameters which we aggregate as a single vector $\vec{\theta}$. The objective was to find a parameter set $\vec{\theta^*}$ that satisfied:

$$\vec{\theta^*} \in \vec{\theta} \quad \text{such that} \quad \text{Min} \sum_{i=1}^{13} \log \left(\frac{y_i^t(\vec{\theta})}{y_i^*} \right)^2 \tag{S41}$$

   where $y^t(\theta)$ is the model output given a candidate parameter set θ and y^* is the vector of target densities, i.e.,

$$y_d^* \equiv (H^*, C^*, E^*, Z^*, V_H^*, V_C^*, V_E^*, x_{on}^*, x_{in}^*, \ldots) \tag{S42}$$

   augmented by four additional features, the ratio of virus to hosts, and the fraction of mortality of H, C and E due to viruses, for a total of 13 targets. The index i denotes one of the 13 components of the model output. The choice of this is meant to weight all output features equally, while balancing deviations on vastly different scales.

The following are the "target" set of densities utilized in this procedure:

$$\begin{aligned}
H^* &= 2 \times 10^8 \\
C^* &= 2 \times 10^8 \\
E^* &= 2 \times 10^6 \\
Z^* &= 5 \times 10^4 \\
V_H^* &= 2 \times 10^9 \\
V_C^* &= 2 \times 10^9 \\
V_E^* &= 2 \times 10^7 \\
x_{on}^* &= 5 \\
x_{in}^* &= 0.1 \\
\text{Ratio of viruses to hosts} &= 10, \\
\text{Fractional mortality due to viruses of } H &= 0.5 \\
\text{Fractional mortality due to viruses of } C &= 0.25 \\
\text{Fractional mortality due to viruses of } E &= 0.1
\end{aligned}$$

Here, the densities are in units of particles/L with the exception of x_{on}^* and x_{in}^* which are in units of μmol/L. The nonlinear optimization process yielded parameter sets, of which the top 5% are seen in Figure 4.

4.3 Sloppy-stiff analysis

Parameters in a model can have substantially different effects on model output. One approach to characterize these effects is via a form of sensitivity analysis termed sloppy-stiff analysis [11, 26]. Parameters which cause large changes to output given small variations in their values are referred to as stiff. In contrast, parameters

which cause small changes to output given small variations in their values are referred to as sloppy. The information necessary to characterize the relative sloppiness and stiffness of all parameters can be derived from a Hessian matrix, where the ij-th element is defined as:

$$\mathcal{H}_{ij} = \sum_n \frac{\partial \log y_n}{\partial \log \theta_i}\bigg|_{\vec{\theta}^*} \frac{\partial \log y_n}{\partial \log \theta_j}\bigg|_{\vec{\theta}^*} = \sum_n \frac{\theta_i^* \theta_j^*}{(y_n^*)^2} \frac{\partial y_n}{\partial \theta_i}\bigg|_{\vec{\theta}^*} \frac{\partial y_n}{\partial \theta_j}\bigg|_{\vec{\theta}^*}. \tag{S43}$$

There are n total variables in the model and the reference parameters are represented by a vector $\vec{\theta}$. The bar notation emphasizes that the partial derivatives are evaluated at the reference parameter set. The argument of the sum is made unitless by a prefactor involving the reference parameter set, $\vec{\theta}^*$ and the respective equilibrium values of the variables, $\vec{y}^*$. Each element of the Hessian is interpreted as the sum of the relative changes of each variable due to relative changes of the respective parameters. Here, we considered perturbations to all parameters except p_g, p_{on}, and p_{in} due to the algebraic constraint restricting their values to a subspace. Moreover, we focus the sloppy-stiff analysis on the reference parameter set associated with the lowest deviation from the target densities.

Eigenvalues of the Hessian quantify the total amount of change to all variables given a perturbation to a combination of parameters defined by the respective eigenvector. The eigenvalue spectrum shows that perturbations to some combinations of parameters cause a majority of the effect on variables (Figure S6). Each eigenvalue corresponds to some combination of parameters. In our case, the eigenvalue spectrum is dominated by the principle eigenvalue. To get a sense of which parameters are stiff and sloppy We compute the orientation of the principle eigenvector in parameter space to identify those parameters that are most "stiff" (Figure S7). For this reference set and metric of perturbations, small values associated with the cyanobacteria processes and with zooplankton respiration are predicted to have the largest effect on output.

References

[1] S. B. Baines and M.L. Pace. The production of dissolved organic matter by phytoplankton and its importance to bacteria: patterns across marine and freshwater systems. *Limnology and Oceanography*, 36:1078–1090, 1991.

[2] S. Bertilsson, O. Berglund, D. M. Karl, and S. W. Chisholm. Elemental composition of marine Prochlorococcus and Synechococcus: Implications for the ecological stoichiometry of the sea. *Limnology and Oceanography*, 48:1721–1731, 2003.

[3] Chris M. Brown, Janice E. Lawrence, and Douglas A. Campbell. Are phytoplankton population density maxima predictable through analysis of host and viral genomic DNA content ? *J. Mar. Biol. Assn. U. K.*, 86:491–498, 2006.

[4] J. R. Christian and T. R. Anderson. Modeling DOM biogeochemistry. In D. A. Hansell and C. A. Carlson, editors, *Biogeochemistry of marine dissolved organic matter*, pages 717–755, New York, 2002. Academic Press.

[5] Marianne De Paepe and François Taddei. Viruses' life history: towards a mechanistic basis of a trade-off between survival and reproduction among phages. *PLoS biology*, 4:e193, 2006.

[6] Paul A. del Giorgio and Jonathan J. Cole. Bacterial growth efficiency in natural aquatic systems. *Annual Review of Ecology and Systematics*, 29(1):503–541, 1998.

[7] H. W. Ducklow. Bacterial production and biomass in the oceans. In D. L. Kirchman, editor, *Microbial Ecology of the Oceans*, pages 85–120, New York, 2000. John Wiley and Sons.

[8] Kyle F. Edwards, Mridul K. Thomas, Christopher a. Klausmeier, and Elena Litchman. Allometric scaling and taxonomic variation in nutrient utilization traits and maximum growth rate of phytoplankton. *Limnology and Oceanography*, 57:554–566, 2012.

[9] R. W. Eppley, J. N. Rogers, and J. J. McCarthy. Half-saturation constants for uptake of nitrate and ammonium by marine phytoplankton. *Limnol. Oceanogr.*, 14:912–920, 1969.

[10] R. J. Geider. Respiration: taxation without representation. In P. G. Falkowski, A. D. Woodhead, and K. Vivirito, editors, *Primary Productivity and Biogeochemical Cycles in the Sea*, New York, 1992. Plenum Press.

[11] Ryan N Gutenkunst, Joshua J Waterfall, Fergal P Casey, Kevin S Brown, Christopher R Myers, and James P Sethna. Universally sloppy parameter sensitivities in systems biology models. *PLoS Comput Biol*, 3:e189, 2007.

[12] P. J. Hansen, P. K. Bjornsen, and B. W. Hansen. Zooplankton grazing and growth: scaling within the 2-2000-mm body size range. *Limnology and Oceanography*, 42:687–704, 1997.

[13] Luis F Jover, T. Chad Effler, A. Buchan, Steven W. Wilhelm, and Joshua S. Weitz. The elemental composition of virus particles: implications for marine biogeochemical cycles. *Nature Reviews Microbiology*, 12:519–528, 2014.

[14] C A Klausmeier, E Litchman, and S A Levin. Phytoplankton growth and stoichiometry under multiple nutrient limitation. *Limnology and Oceanography*, 49:1463–1470, 2004.

[15] Elena Litchman, Christopher A. Klausmeier, Oscar M. Schofield, and Paul G. Falkowski. The role of functional traits and trade-offs in structuring phytoplankton communities: scaling from cellular to ecosystem level. *Ecology Letters*, 10(12):1170–1181, 2007.

[16] M. D McKay, R. J. Beckman, and W. J Conover. A comparison of three methods for selecting values of input variables in the analysis of output from a computer code. *Technometrics*, 21:239–245, 1979.

[17] Takeshi Miki, Takefumi Nakazawa, Taichi Yokokawa, and Toshi Nagata. Functional consequences of viral impacts on bacterial communities: a food-web model analysis. *Freshwater Biology*, 53:1142–1153, June 2008.

[18] A. G. Murray and G. A. Jackson. Viral dynamics: a model of the effects of size, shape, motion and abundance of single-celled planktonic organisms and other particles. *Marine Ecology Progress Series*, 89:103–116, 1992.

[19] T Nagata. Production mechanisms of dissolved organic matter. In D.L. Kirchman, editor, *Microbial Ecology of the Oceans*, pages 121–152, New York, 2000. John Wiley and Sons, Inc.

[20] P Parada, Gerhard J Herndl, and Markus G Weinbauer. Viral burst size of heterotrophic prokaryotes in aquatic systems. *J. Mar. Biol. Ass. UK*, 86:613–621, 2006.

[21] Géraldine Sarthou, Klaas R. Timmermans, Stéphane Blain, and Paul Tréguer. Growth physiology and fate of diatoms in the ocean: a review. *Journal of Sea Research*, 53:25 – 42, 2005. Iron Resources and Oceanic Nutrients - Advancement of Global Environmental Simulations.

[22] C Stock and J Dunne. Controls on the ratio of mesozooplankton production to primary production in marine ecosystems. *Deep Sea Research I*, 57:95 – 112, 2010.

[23] D. Straile. Gross growth efficiencies of protozoan and metazoan zooplankton and their dependence on food concentration, predator-prey weight ratio, and taxonomic group. *Limnology and Oceanography*, 42:1375–1385, 1997.

[24] Curtis A. Suttle. Marine viruses - major players in the global ecosystem. *Nature Reviews Microbiology*, 5:801–812, OCT 2007.

[25] Curtis A Suttle and Feng Chen. Mechanisms and rates of decay of marine viruses in seawater. *Appl. Env. Micro.*, 58:3721–3729, 1992.

[26] Bradford Taylor, Tae J. Lee, and Joshua S. Weitz. A guide to sensitivity analysis of quantitative models of gene expression dynamics. *Methods*, 62(1):109 – 120, 2013.

[27] T. F. Thingstad. Elements of a theory for the mechanisms controlling abundance, diversity, and biogeochemical role of lytic bacterial viruses in aquatic systems. *Limnology and Oceanography*, 45:1320–1328, 2000.

[28] Richard G. Williams and Michael J. Follows. *Ocean Dynamics and the Carbon Cycle Principles and Mechanisms*. Cambridge University Press, Cambridge, UK, 2011.

[29] Erik R. Zinser, Debbie Lindell, Zackary I. Johnson, Matthias E. Futschik, Claudia Steglich, Maureen L. Coleman, Matthew A. Wright, Trent Rector, Robert Steen, Nathan McNulty, Luke R. Thompson, and Sallie W. Chisholm. Choreography of the transcriptome, photophysiology, and cell cycle of a minimal photoautotroph, *Prochlorococcus*. *PLoS ONE*, 4(4):e5135, 04 2009.

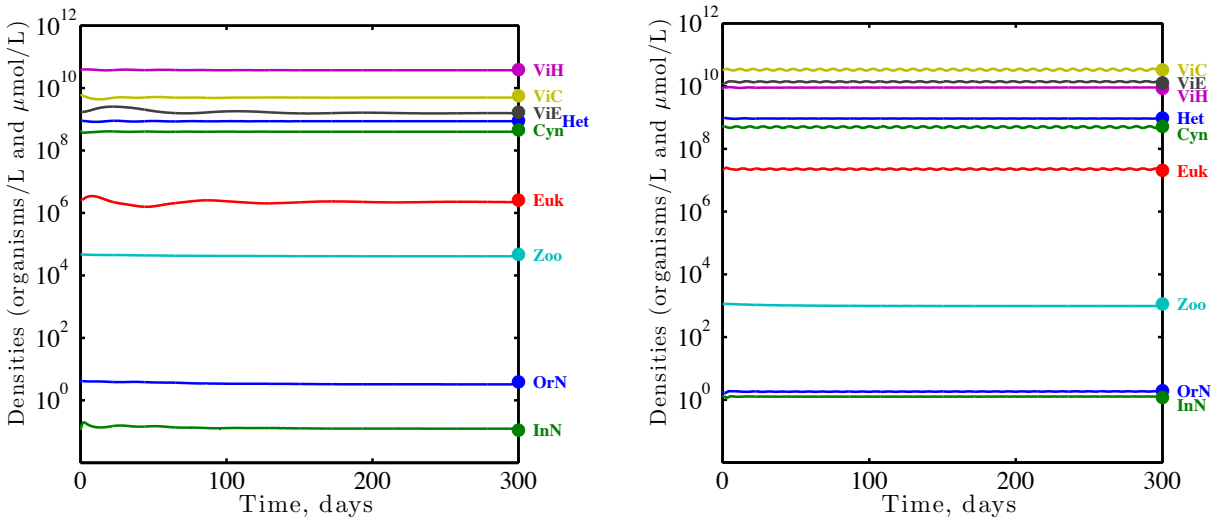

Figure S1: Dynamics of the model near putative steady states. (A) Dynamics shown to asymptotically converge to steady state. (B) Dynamics shown to diverge from a steady state leading to a limit cycle. In both cases, filled circles denoted at 300 days denote predicted equilibrium values of populations and nutrients, given parameters listed in Supplementary Table S1.

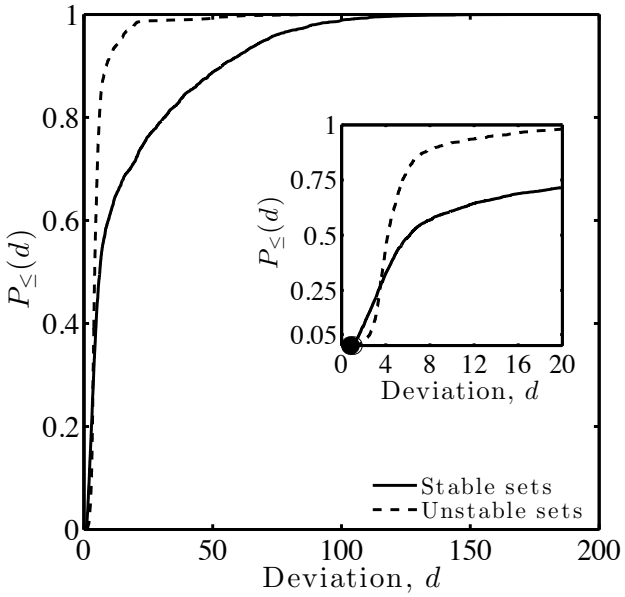

Figure S2: Cumulative distributions, $p_{\leq}(d)$, of deviations d from the target set of 13 densities and indices associated with equilibria of the multi-trophic ecosystem model (see text for main details). Distributions are associated with fixed points that are stable (solid line) or unstable (dashed line). The inset focuses on deviations $d \leq 20$, where it is evident that smaller deviations are associated with fixed points that are stable. 94% of the top 5% of parameters sets corresponded to equilibrium that were locally stable. Further, we find that the distribution of deviations associated with stable and unstable fixed points are significantly unequal ($p \ll 10^{-10}$). In particular, as is evident in Figure S2, the cumulative distribution of the deviations, d, has significantly greater mass at low values of d for equilibria associated with stable fixed points than it does for those associated with unstable fixed points.

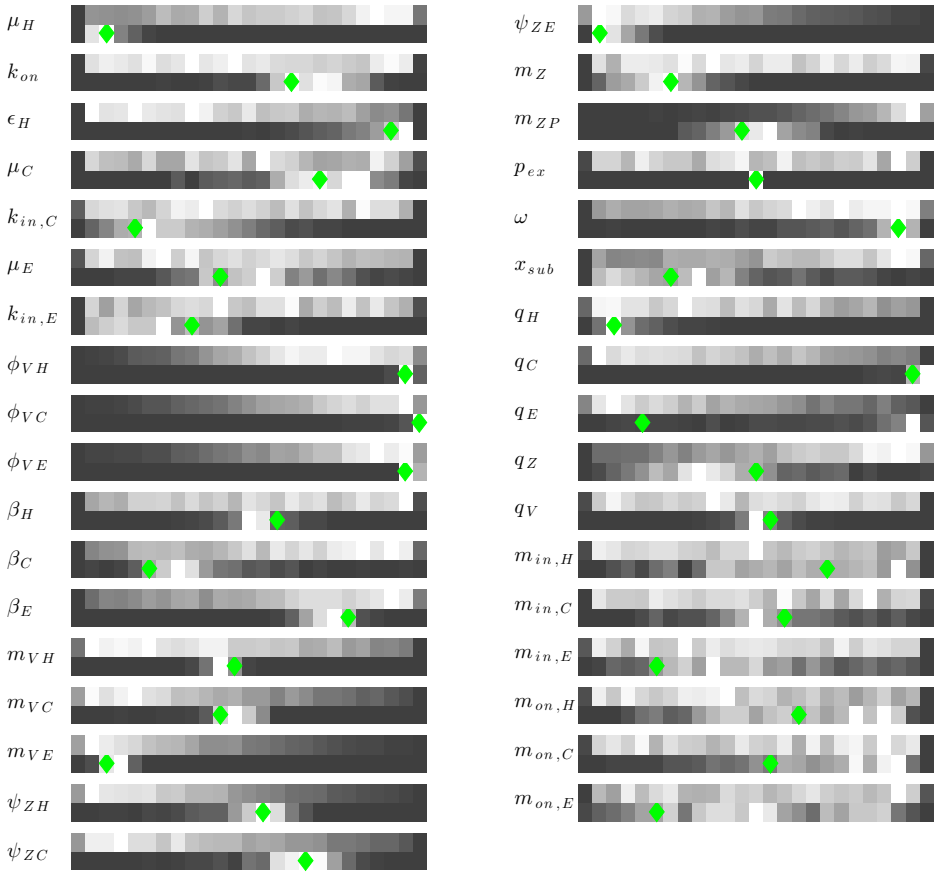

Figure S3: Distributions of parameter values obtained via nonlinear optimization. The distribution correspond to the top 5% of model feature output. The barcodes represent intensity histograms (white denotes greater number of replicates). There are two "barcodes" associated with each parameter. The top barcode corresponds to the distribution of parameters associated with feasible parameter sets obtained via the LHS sampling. The bottom barcode corresponds to the distribution of parameters in the targeted parameter sets obtained via nonlinear optimization. The green diamond denotes the value of the parameter associated with the best hit model replicate.

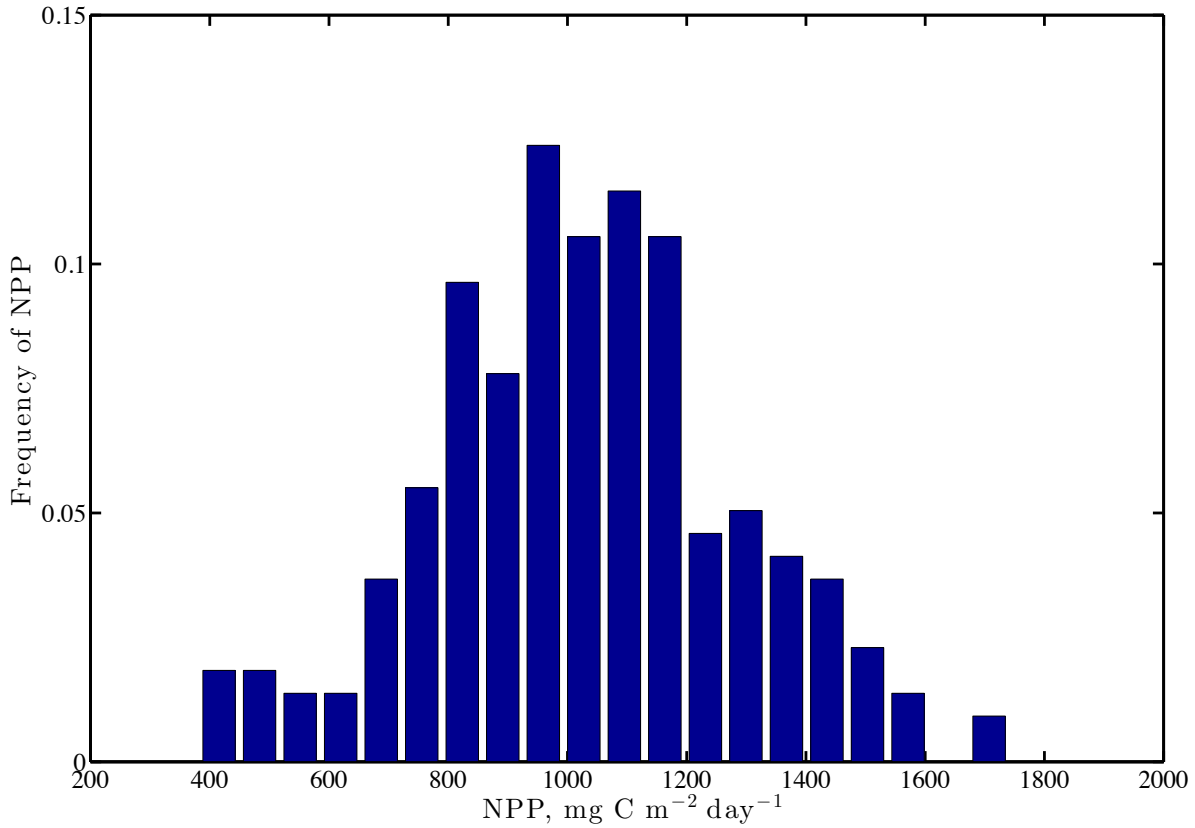

Figure S4: NPP for the top 5% of model replicates. NPP in units of mg C m^{-2} days^{-1} was calculated by multiplying the total net primary productivity in units of μmol N L^{-1} days^{-1} by the conversion factors (106/16) (denoting a baseline C:N ratio), 25 m (denoting a euphotic zone, above the nutricline), and 12.01 (denoting g C per mole). Note that moving from μmol to mmol and L to m^3 involving canceling factors of 1000. The NPP has a mean of 1030 with a standard deviation of 260.

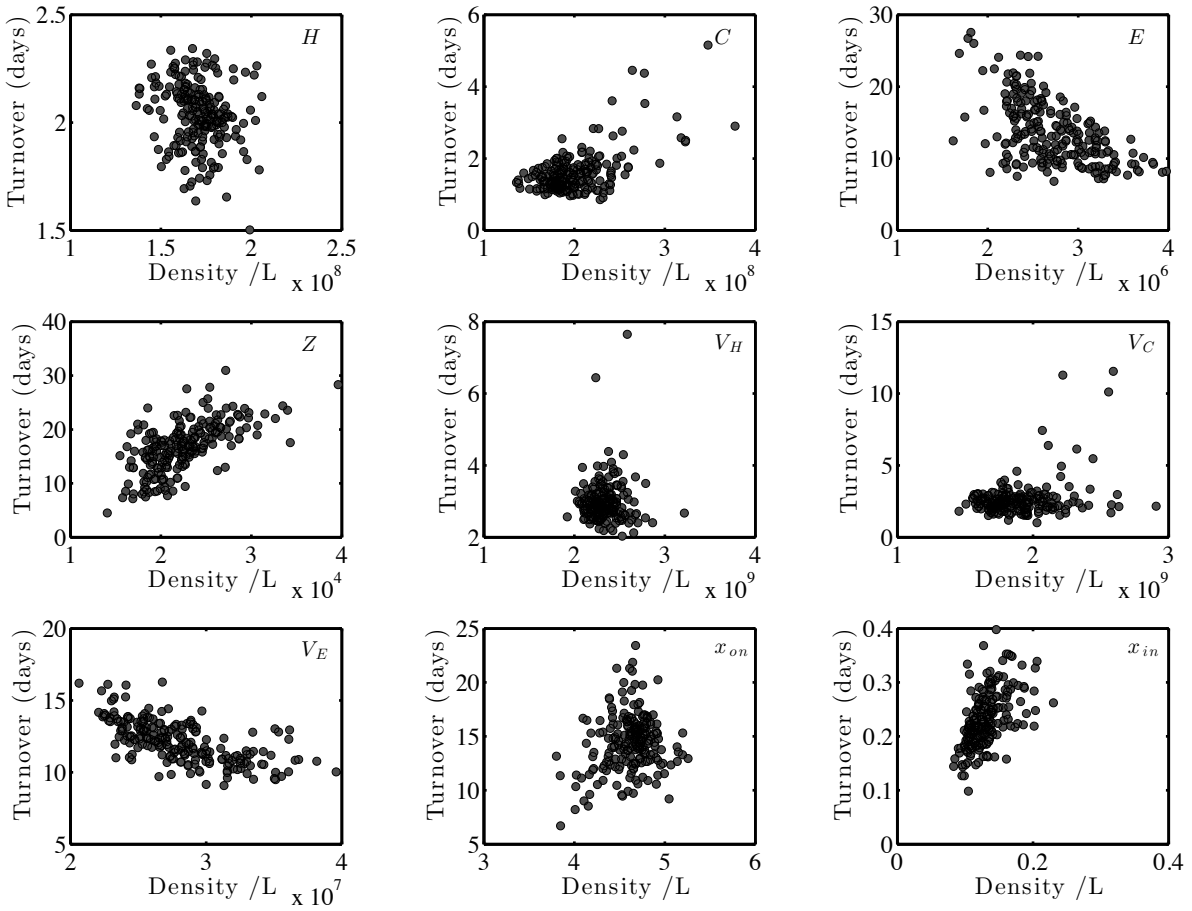

Figure S5: Turnover time, in days, for all dynamic variables, as estimated for the targeted parameter sets. In general, given a nonlinear dynamical system of the form $\dot{x} = a - kx$ where a is an input rate and k is a turnover rate, the expectation is that the variable x has a residence time (or equivalently, turnover time) of $\tau = 1/k$. Note that the equilibrium, $x^* = a/k$. Hence, the turnover time can be estimated based on the loss rate $\tau_- = \frac{x^*}{kx^*} = \frac{1}{k}$ or the input rate $\tau_+ = \frac{x^*}{a} = \frac{a}{ak} = \frac{1}{k}$. These must be equal at equilibrium as inputs balance losses. We apply this same principle to estimate the turnover time for each of the nine variables in the model. In each case, the dynamical system in Eqs. (A1-A9) can be separated into input terms, I, and loss terms, D. Then, for each equilibrium $x^*(\theta)$ associated with a parameter set θ, the turnover time was estimated at the equilibrium.

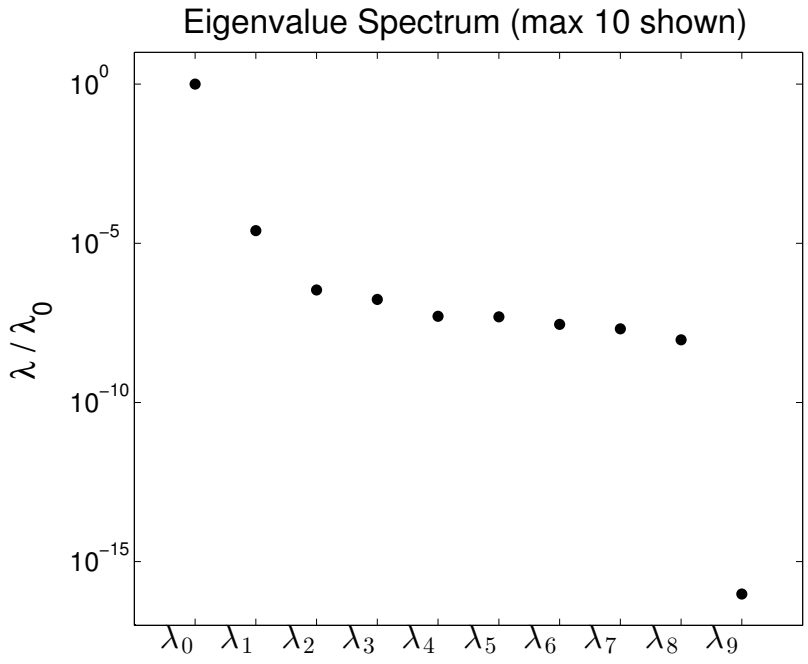

Figure S6: Eigenvalue Spectrum of parametric Hessian matrix. Values are normalized relative to the principle eigenvalue. Only the first 10 eigenvalues of the spectrum are shown. Note that the most of the perturbations in model output are due to deviations along a single, principle eigenvector, associated with the principle eigenvalue. Analysis done by considering perturbations to all parameters except p_g, p_{on}, and p_{in}.

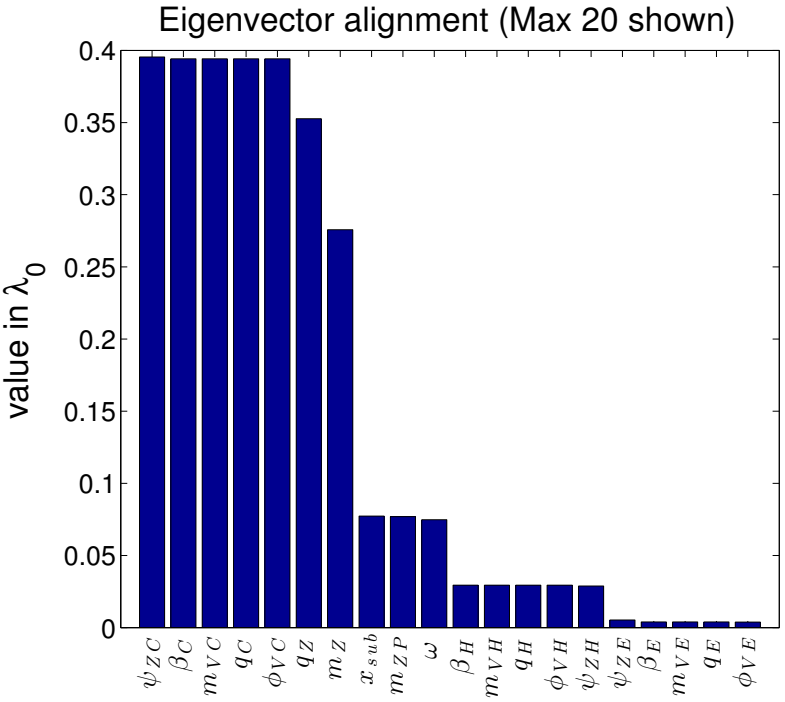

Figure S7: Projection of biological parameters along the principle eigenvector. The higher values correspond to stiffer parameters. Only the 20 stiffest parameters are shown. Analysis done by considering perturbations to all parameters except p_g, p_{on}, and p_{in}.

Event	Variable	Meaning	Units	Attracting	Limit cycle
H growth	μ_H	Max H growth rate	day^{-1}	0.51	0.61
	K_{on}	Half-saturation constant	μmol/L	0.94	0.68
	ϵ_H	Efficiency	N/A	0.20	0.19
C growth	μ_C	Max C growth rate	day^{-1}	1.97	0.68
	$K_{in,C}$	Half-saturation constant	μmol/L	0.053	0.059
E growth	μ_E	Max E growth rate	day^{-1}	7.5	5.4
	$K_{in,E}$	Half-saturation constant	μmol/L	5.4	5.8
Viral lysis	ϕ_{VH}	Lysis rate	L/(virus·day)	8.0×10^{-12}	4.3×10^{-11}
	ϕ_{VC}	Lysis rate	ibid	9.9×10^{-11}	1.9×10^{-11}
	ϕ_{VE}	Lysis rate	ibid	5.8×10^{-11}	6.7×10^{-11}
	β_H	Burst size	N/A	25	15
	β_C	Burst size	N/A	16	82
	β_E	Burst size	N/A	440	370
Viral decay	m_{VH}	Decay rate	day^{-1}	0.17	0.59
	m_{VC}	Decay rate	day^{-1}	0.63	0.76
	m_{VE}	Decay rate	day^{-1}	0.058	0.56
Zooplankton grazing	ψ_{ZH}	Grazing rate	L/(zoopl·day)	1.9×10^{-6}	2.2×10^{-5}
	ψ_{ZC}	Grazing rate	ibid	2.1×10^{-5}	4.2×10^{-5}
	ψ_{ZE}	Grazing rate	ibid	1.5×10^{-6}	2.8×10^{-5}
	p_g	Fraction for growth	N/A	0.4	0.4
	p_{on}	Fraction egested	N/A	0.3	0.3
	p_{in}	Fraction respired	N/A	0.3	0.3
Grazer respiration	m_Z	Basal respiration	day^{-1}	0.048	0.051
Consumption by higher predators	m_{ZP}	Mortality rate	L/(cells·day)	3.3×10^{-7}	2.8×10^{-5}
	p_{ex}	Fraction exported	N/A	0.49	0.37
Import	ω	Surface-deep mixing rate	1/day	0.016	0.077
	x_{sub}	Deep inorganic N conc.	μmol N/L	7.7	2.67
Nutrient levels	q_H	Nitrogen content of H	μmol N/cell	8.8×10^{-10}	1.4×10^{-9}
	q_C	Nitrogen content of C	ibid	3.9×10^{-9}	3.0×10^{-9}
	q_E	Nitrogen content of E	ibid	2.1×10^{-7}	6.7×10^{-8}
	q_Z	Nitrogen content of Z	ibid	2.3×10^{-4}	3.9×10^{-4}
	q_V	Nitrogen content of V	ibid	2.0×10^{-12}	2.2×10^{-12}
Cellular loss	$m_{in,H}$	H respiration	day^{-1}	0.0069	0.0067
	$m_{in,C}$	C respiration	day^{-1}	0.0050	0.016
	$m_{in,E}$	E respiration	day^{-1}	0.0043	0.0023
	$m_{on,H}$	H organic loss	day^{-1}	0.014	0.034
	$m_{on,C}$	C organic loss	day^{-1}	0.022	0.0063
	$m_{on,E}$	E organic loss	day^{-1}	0.011	0.022

Table S1: Parameters used in simulations of Figure S1A (attracting) and Figure S1B (limit cycle) ecosystem dynamics.

Event	Variable	Meaning	Units	Lower Bound	Upper bound
H growth	μ_H	Max H growth rate	day^{-1}	0.50	2
	K_{on}	Half-saturation constant	μmol/L	0.25	1
	ϵ_H	Efficiency	N/A	0.05	0.2
C growth	μ_C	Max C growth rate	day^{-1}	0.5	2
	$K_{in,C}$	Half-saturation constant	μmol/L	0.05	1
E growth	μ_E	Max E growth rate	day^{-1}	0.2	2
	$K_{in,E}$	Half-saturation constant	μmol/L	0.5	10
Viral lysis	ϕ_{VH}	Lysis rate	L/(virus·day)	10^{-13}	10^{-10}
	ϕ_{VC}	Lysis rate	ibid	10^{-13}	10^{-10}
	ϕ_{VE}	Lysis rate	ibid	10^{-12}	10^{-10}
	β_H	Burst size	N/A	12.5	50
	β_C	Burst size	N/A	12.5	100
	β_E	Burst size	N/A	125	500
Viral decay	m_{VH}	Decay rate	day^{-1}	0.05	5
	m_{VC}	Decay rate	day^{-1}	0.05	5
	m_{VE}	Decay rate	day^{-1}	0.05	5
Zooplankton grazing	ψ_{ZH}	Grazing rate	L/(zoopl·day)	10^{-6}	10^{-4}
	ψ_{ZC}	Grazing rate	ibid	10^{-6}	10^{-4}
	ψ_{ZE}	Grazing rate	ibid	10^{-6}	10^{-4}
	p_g	Fraction for growth	N/A	0.4	0.4
	p_{on}	Fraction egested	N/A	0.3	0.3
	p_{in}	Fraction respired	N/A	0.3	0.3
Grazer respiration	m_Z	Basal respiration	day^{-1}	0.025	0.1
Consumption by higher predators	m_{ZP}	Mortality rate	L/(cells·day)	10^{-8}	10^{-4}
	p_{ex}	Fraction exported	N/A	0.25	1
Import	ω	Surface-deep mixing rate	1/day	0.005	0.02
	x_{sub}	Deep inorganic N conc.	μmol N/L	2.5	10
Nutrient levels	q_H	Nitrogen content of H	μmol N/cell	5×10^{-10}	4×10^{-9}
	q_C	Nitrogen content of C	ibid	5×10^{-10}	4×10^{-9}
	q_E	Nitrogen content of E	ibid	5×10^{-8}	4×10^{-7}
	q_Z	Nitrogen content of Z	ibid	5×10^{-5}	4×10^{-4}
	q_V	Nitrogen content of V	ibid	0.5×10^{-12}	20×10^{-12}
Cellular loss	$m_{in,H}$	H respiration	day^{-1}	0.001	0.1
	$m_{in,C}$	C respiration	day^{-1}	0.001	0.1
	$m_{in,E}$	E respiration	day^{-1}	0.001	0.1
	$m_{on,H}$	H organic loss	day^{-1}	0.005	0.1
	$m_{on,C}$	C organic loss	day^{-1}	0.005	0.1
	$m_{on,E}$	E organic loss	day^{-1}	0.005	0.1

Table S2: Parameter ranges used for LHS sampling of initial parameters.